In vitro study of Biodegradation in Mg-alloys by Isothermal Calorimetry

Akshat Kulkarni Prasad Kekare

2021

LUND UNIVERSITY

LTH

FACULTY OF ENGINEERING

MASTER'S THESIS
DIVISION OF MATERIALS ENGINEERING
LUND UNIVERSITY

Supervisor: Dmytro Orlov, Professor

Co-Supervisor: Lars Wadsö, Professor: Division of Building Materials

Examiner: Srinivasan Iyengar, Professor

MSC Thesis

ISBN LUTFD2/TFMT--21/5065--SE

Author: Akshat Kulkarni and Prasad Kekare
Lund, Sweden 2021

Avdelningen för mateiralteknik
Lunds Tekniska Högskola
Lunds universitet
Box 118
221 00 Lund
Sverige

Division Materials Engineering
LTH, School of Engineering
Lund University
Box 118
SE-221 00 Lund
Sweden

Printed in Sweden.
Media-Tryck
Lund University

Foreword

Firstly, we would like to thank our supervisor, Professor Dmytro Orlov, for giving us an opportunity to work on this wonderful project. And we are grateful to him for providing us with a new pathway in the critical field of corrosion science.

We would like to express our sincere gratitude to our Examiner Professor Emeritus Srinivasan Iyengar, for taking time out of his busy schedule and reviewing our work.

Professor Lars Wadsö was very generous in helping us with instrumentation knowledge related to Isothermal Calorimeter and Data Processing.

We had a fantastic experience and a long learning journey with Zoran Markovski, and we would like to appreciate his efforts in being with us during our project.

The journey was exhilarating and sometimes exasperating as well but our friends Venkatesh Pottabathini and Supradeepa Panual constantly encouraged us and provided some great inputs in managing the data as well.

This journey would not have happened without support of our parents. We look up to them as source of our inspiration and will continue to rise to their expectation and fulfill our endeavors in academic life.

Lund 2021–06-12

Akshat Kulkarni and Prasad Kekare

Abstract

Magnesium corrosion in an aqueous environment is a multi-layer, complex process. A literature survey shows significant gaps and the modelling work reported indicates lack of clarity in understanding the corrosion process. Studies on the effects of impurities and interfacial compounds formed by selected alloying additions would help in filling some of these gaps.

Further, the evolution of hydrogen gas with the dissolution magnesium may pose a threat to living cells in Biomedical Applications. As a result, it is critical to monitor Mg corrosion rates and investigate the impact of alloying elements. For clarity, an overview of the basic mechanisms of magnesium corrosion in a aqueous solution and the thermodynamic background is presented.

The project investigates the corrosion behaviour of three alloys (Mg-0.8Nd, Mg-0.2Zr & Mg-0.8Nd-0.2Zr) in a 0.9wt% NaCl solution using Isothermal calorimetry and the pressure measurement technique. Heat flow, and energy changes were monitored, providing the basis for understanding the corrosion process. Hydrogen gas evolution measurements were correlated with thermal power. Small changes in the corrosion process lead to noise-like variations in thermal power. The effect of alloying addition and heat treatment on corrosion rates have also been addressed in the present study.

Keywords: Isothermal Calorimetry, Degradation of Mg Alloys, Supersaturated solid solution (SSSS), Corrosion rate, Aqueous corrosion.

Table of Contents

List of figures:

List of Tables:

Introduction:

Considerable research is currently focusing on the development of magnesium alloys with attractive properties like light weight and high specific strength. This development is being driven by the recognition that there is an urgent need for developing light components, which are critical in meeting the demands of energy efficient transport. This approach can be seen in the efforts to find compatible replacements for the currently used biomedical implants, especially with the increase in bone fractures and injuries due to sport activities, as well as accidents. The biodegradable implant material dissolves gradually inside the human body fluids with simultaneous regeneration of the surrounding bone tissues. Furthermore, the conventional implant materials require additional surgical intervention for removal and often result in inflammation and irritation. The conventional materials used for implants mainly steel, titanium and cobalt chromium alloys have a high elastic modulus (100GPa to 200GPa) as compared to the cortical bone(40Gpa) and may result in weakening of the bone as most of the stress is carried by the implant. This effect also knows as stress shielding is detrimental for bone healing. Thus, a need for developing a material which can help in healing and dissolve gradually with controlled corrosion rate is imperative.

Magnesium was selected as a potential material for biodegradable implant since it is nontoxic and highly inert and compatible with human body. Also, the Mg^{2+} ions are inherently present in human body and help in carrying out metabolic reactions. Despite of the advantages and possible applications, the corrosion rates observed for magnesium alloy in aqueous solution formed a barrier for its potential usage as biodegradable implant material.

Magnesium corrodes rapidly in aqueous solutions, while its reaction with water involves generation of $Mg(OH)_2$ and MgO films which are quite unstable, the chloride ions in human body accelerates the corrosion by formation of highly soluble magnesium chloride. The critical concentration of chloride ions detrimental to Mg can be found

in work done by (BA., 2003). The addition of alloying elements improves the mechanical and physical properties of Magnesium, nonetheless it also affects the oxidation behaviour as they form secondary phases in the primary matrix. The solid solubility of alloying elements in Magnesium is relatively less and the detailed data can be found in appendix. Decrease in solid solubility of these elements during conventional casting process leads to formation of primary precipitates which act as cathode relative to primary Mg matrix. Thus, the microstructural effect on corrosion behaviour of magnesium alloys is an important topic but it is not studied in the present work due to limited scope. In the present work the corrosion behaviour of three model Mg alloys (Mg-0.8Nd, Mg-0.2Zr & Mg-0.8Nd-0.2Zr) is analysed in 0.9wt% NaCl solution at 37^0C mimicking human body conditions. Also, the effect of solid solution heat treatment on corrosion rate is presented for comparison and analysis. A multimodal technique involving combination of Iso thermal calorimetry and gravimetric pressure measurement is utilized for analysing the corrosion behaviour of selected Mg alloy samples. This novel technique developed at Lund University provided two independent sources for corrosion rate monitoring as well as process kinetics. The methodology and principle of operation is explained in detail in subsequent sections.

Objectives:

The primary goal of this research is to study the corrosion behaviour of three representative model Mg alloys in an aqueous medium closely resembling the physiological condition.

- The effect of alloying additions and heat treatment on corrosion rate of selected Mg alloys (Mg-0.8Nd, Mg-0.2Zr & Mg-0.8Nd-0.2Zr) is investigated.
- A novel technique combining Isothermal calorimetry and pressure measurement is used as an analytical tool in the investigation.
- Scanning electron microscopy is used as a main analytical to study the morphology of the corroded film.

1. Literature Review and Theory:

1.1. Background:

1.1.1. Developments and insights into Magnesium corrosion

The Early discovery of the Magnesium as an element was made by Scottish physician Joseph Black in 1755 (Kammer, 2000), while the metallic Mg was isolated by Davy in 1808. The corrosion behaviour of Magnesium in moist air was first reported by Bussey in 1831. His experimental investigation confirmed the evolution of hydroxide film as Magnesium was exposed to moist air. Furthermore, the influence of aqueous medium on corrosion behaviour of Magnesium was analyzed by (W.Beetz, 1866) which was first reported study confirming hydrogen evolution with dissolution of Magnesium. The corrosivity of Magnesium while considering its biodegradable properties was first studied by (Witte, 2010). These early developments and understanding of corrosion behaviour of Magnesium has been tremendously instrumental in designing new alloys, Also the experimental evidence of hydrated layer of oxide in aqueous solution and evolution of hydrogen gas as reported in earl1920's's is the basis for the current work and could be seen in the subsequent sections.

1.1.2. Basic Overview of Magnesium-Alloys in Medical Applications:

Magnesium alloys find a potent application in biomedical field, especially in orthopaedic surgeries where hip joints, screws, bone plates and stents are implanted inside the human body. These applications demand certain conditions to bet met for human body to be conducive to the implant material. The first condition is human body should coexist with selected implant material without any significant change to the surrounding tissue or the material itself. Furthermore, there should not be an inflammation to the bone tissue form the implant material, (Mirco Peron, 2017). Titanium and steel implants find majority of the applications but there are certain drawbacks to their use. Second surgery is needed sometimes to remove them, and their elastic modulus and yield strength are high as

compared to the cortical human bone. The phenomenon also called as stress shielding result from these large differences in mechanical properties of implant material and human bone. This leads to stress re-distribution around the bone and implant material and if the difference is too high, the bone will become porous or the implant material will fail according to the wolf's law, (Wolffe, 1986). Fig (1) shows stress shielding effect and weakening of bone. Thus, Magnesium was selected for evaluation as it has similar yield strength and modulus compared to human bone and degrades at the same time avoiding a possibility of implant removal. However spontaneous degradation of Mg alloys poses a problem, although its ability to self-degrade is exploited. It is a double-edged sword as the reaction of Mg with physiological fluids might be detrimental to the surrounding bone tissues and human health. Although a surge in developing Mg alloys for bio medical applications is a relatively recent phenomenon, a very old study dating back to 1878 was made on use of Mg wires as ligature for bleeding vessels, (Witte, 2010) . The early investigative reports on potential use of mg alloys in bio medical applications were in preliminary stages due to limited understanding in corrosion behaviour of Mg. In the present study corrosion behaviour of selected Mg alloys is analysed to address the significant gaps in the literature.

The principal application in biomedicine is as a biodegradable implant material. Currently, most screw and plate implants used to treat bone fractures are made of titanium alloys or steels. Not only do these materials produce harmful metal particles when they corrode, but the surrounding bone tissue is weakened by a process known as" "stress shielding" due to their comparatively high stiffness compared to natural bone. On the other hand, Magnesium has an elastic modulus that is much closer to that of bones, which helps to reduce this effect. (Staiger et al., 2006).

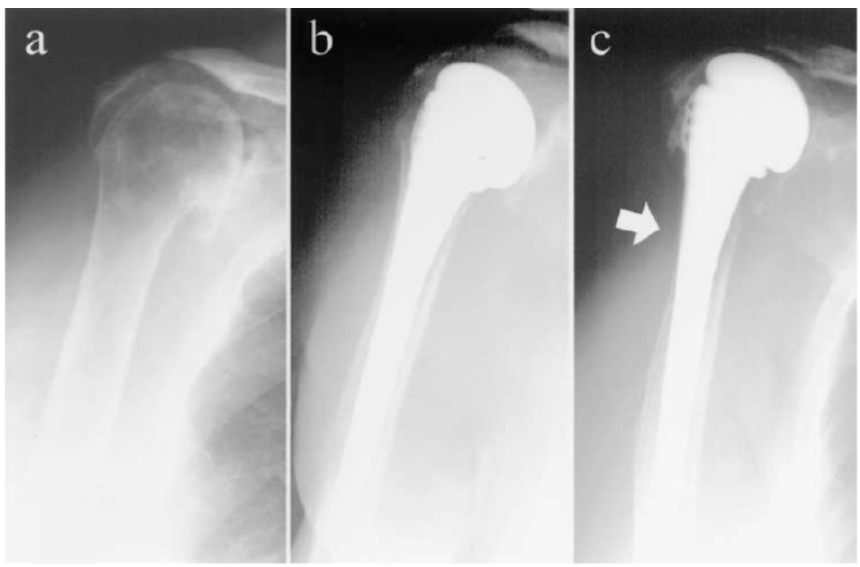

Figure 1 Stress shielding effect showing weakening of bone in shoulder replacement surgery after 7 years; a) pre-operative image; b) image taken after surgery, (Nagels, 2003)

Magnesium is non-toxic and can stimulate the formation of bone tissue in the human body after implantation. Mg and some of its alloys have biodegradable implant applications that are promising. Unfortunately, the Mg alloys of today degrade rapidly in the human body's electrolyte environment, which impairs the mechanical integrity of the Mg alloy implant, leading to implant failure before the host tissue has healed sufficiently. Corrosion causes a gradual loss in both the structural integrity and the mass of the Mg alloys. An additional worry with the use of Mg alloy implants is hydrogen gas generation due to corrosion in vivo. When magnesium alloys corrode rapidly in a physiological environment, large amounts of hydrogen gas is released, posing severe health risks to the human body (Ding et al., 2014).

1.2. Effects of Alloying Elements:

Magnesium is a light metal that corrodes when it comes in contact with an aqueous solution. It has a density of 1.74 g/cm3 at room temperature, which is 1.6 to 4.5 times lower than aluminium or steel. Its appropriate compressive and tensile strengths, as well as its Young's Modulus (41-45 GPa), which is significantly closer to cortical bone than other metallic implant materials, make it an excellent candidate for orthopaedic application. (Ding et al., 2014)

The most common alloying components in Mg alloys are Al, Ca, Zr, and Zn. When these alloying elements react with Mg or with one another, intermetallic phases can form. The microstructural effects, mechanical properties, and corrosion behaviour of intermetallic phases that disperse along grain boundaries or dissolve in the Mg matrix are listed in Table 1.

Some elements, including Mn, Sr, Ce, La, and Nd, have been found to improve the corrosion resistance of Mg alloys. Other elements, such as Ca, Zn, Zr, and Sr, have different effects on corrosion resistance depending on their content: when the content is high, corrosion resistance suffers; when the content is low, corrosion rate slows down. The effects of Nd and Gd on the corrosion of Mg alloys are still relatively unknown, and research based on their influence on corrosion behaviour is controversial. Overall, more research is required to explain the effects of alloying elements on the properties of Mg alloys from the perspective of the corrosion mechanism to provide the comprehensive understanding required to design new Mg alloys alloyed with corrosion-resistant elements (Ding et al., 2014).

Table 1 Influence of alloying elements on the microstructure, mechanical properties, and corrosion:(Ding et al., 2014)

Elements	**Zr**	**Nd**
Effects on microstructure	Excellent grain refining; extremely low solid solubility in pure Mg; excessive use of Zr in Mg alloys should be avoided due to the creation of a stable Mg- Zr phase that degrades the refining grain size; excessive addition leads to rough boundaries.	The refining grain size of Nd-Mg alloys with increasing Nd content.
Effects on mechanical properties	Increasing Zn content somewhat increases ultimate compressive strength; notably improving ductility, elongation, and maximum yield strength of Mg alloys with minor amounts of addition for binary Mg-Zr alloys; usually increasing tensile strength.	Nd content of less than 6%, Nd atoms replace Mg atoms, improving tensile strength and tensile yield strength while decreasing elongation and creep.
Effect on corrosion resistance	Small amounts of Zr addition (less than 2%) improve corrosion resistance; otherwise, corrosion resistance deteriorates dramatically.	$Mg_{12}Nd$ phase suppresses galvanic effect; Nd_2O_3 layer, in addition to pure Mg, effectively enhances corrosion resistance.

1.2.1. Effect of Zr on the Corrosion behaviour of Mg-alloys

Despite its low solubility in the Mg matrix, undissolved Zr particles act as nucleation sites during solidification, resulting in highly fine-equiaxed grains with a distinct hexagonal shape.

Zr is highly resistant to corrosion caused by alkalis, acids, saltwater, and other agents. It has been used to refine grain size and improve corrosion resistance in Mg alloys and other popular alloying elements such as Zn. The protective effect of Zr oxide film (ZrO_2) is another distinguishing feature that makes it appealing. The films formed on binary Mg-Zr alloys after immersion in a borate buffer solution are Zr-Mg double oxyhydroxide enriched with Zr cations. This Zr-Mg double oxyhydroxide acts as a barrier, preventing corrosion of Mg-Zr alloys (Hashimoto et al., 2011).

1.2.2. Effect of Rare-Earth element (REE's) on the Corrosion behaviour of Mg-alloys:

REEs were first isolated as oxides from rare minerals, which are defined as a group of seventeen chemical elements in the periodic table, particularly the fifteen lanthanides, which share chemical properties with scandium (Sc) and yttrium (Y). According to recent research, some REEs in Mg alloying elements have beneficial functions such as improving corrosion resistance, mechanical properties, and electrochemical behaviour due to grain refinement and secondary phase formation (Witte et al., 2010)

Nd is currently widely used in Mg-Zn-Zr-based alloys and Mg-Al-based alloys to improve corrosion resistance and mechanical properties. The second phases of $Mg_{12}Nd$ and $Mg_{41}Nd_5$ are thought to have formed and isolated the Mg matrix, resulting in grain size reduction, and increased tensile strength of Mg alloys. It has been reported that adding Nd to Mg-alloys in concentrations ranging from 1% to 6% reduces grain size while improving tensile and corrosion properties. Furthermore, because the atomic radius difference between Mg and Nd is relatively large, Nd atoms can replace Mg atom positions, posing yet another impediment to dislocation movement. The secondary phases and their distribution along the grain boundaries have been shown to have a significant impact on corrosion in Mg alloys containing Nd. Nd significantly refined the grain size and improved both the tensile and corrosion resistance properties. The alloy with a 6% addition had the best tensile properties and corrosion resistance (Ding et al., 2014).

1.3. Degradation of Mg-Alloys:

The corrosion of Magnesium and its alloys is essentially an electrochemical process and thus the oxidation resistance or characteristics of corrosion are dependent on their electrochemical behaviour. The electrochemical reactions of pure Mg with water and their thermodynamics forms the basis for understanding corrosion behaviour of Magnesium. The information about corrosion rate is not discerned by the thermodynamics but need kinetics to obtain relevant data, Nonetheless the theory behind magnesium corrosion is explained

in the subsequent section while corrosion rate measurement is the actual experimental work involved in this study.

1.3.1. Corrosion characteristics of pure Magnesium:

Like all metals and alloys, Magnesium gets its corrosion control through a natural film on the surface. The content of this film, however, remains unexplained. Films that feature good passive traits include those that limit the outward flow of cations, prohibit the inward flow of damaging anions, and rapidly repair any breakdowns. Passive films protect against several environmental factors and metallurgical impurities, such as electrolyte species and contaminants in the metal (Henry Hu et al., 2014).

1.3.1.1. Environmental effects on Mg:

Any material does not demonstrate corrosion resistance in all environments. Some specific environments are resistant to corrosion, regardless of the materials used. Magnesium has certain environments in which it preferentially operates. Nonetheless, compared to other materials, such as steel and aluminium alloys, fewer medias are suitable for magnesium and magnesium alloys. For example, magnesium and magnesium alloys are typically stable when dissolved in a basic solution, but they dissolve rapidly in neutral and acidic environments. Aluminium alloys are usually stable in neutral media but are unstable in basic and acidic solutions are quite different from the metal alloy (Ferrando, 1989).

1.3.2. General corrosion in aqueous solutions:

Pure Magnesium does not corrode readily at room temperature, with a few exceptions unless the water is present. Magnesium dissolution in liquid or aqueous environments is usually accomplished through an electrochemical reaction with water, which results in magnesium hydroxide and hydrogen gas. Although oxygen is a significant factor in atmospheric corrosion, such a mechanism is largely indifferent to its concentration (Makar et al., 1993). Thermodynamically Mg is very active, and the oxidation reactions mentioned below show the negative Gibbs free energy change for the

reactions. Thus, Mg has natural tendency to spontaneously transform to its oxide state. The oxidized state of Magnesium viz;- Mg2+, MgO & $Mg(OH)_2$ is more stable than the elemental form as it has much more negative chemical potential. The thermodynamic data for the oxidized species and compounds shown in table below confirms the spontaneous corrosion behaviour in aqueous environment,

Reaction 1 describes the probable overall reaction:

$$Mg_{(s)} + 2H_2O_{(l)} \rightarrow Mg(OH)_{2(s)} + H_{2(g)}, \Delta H^{\circ}\text{=-353.01 kJ/mol} \quad (1)$$

This net reaction can be expressed as the sum of the following partial reactions:

Anodic reaction: $Mg \rightarrow Mg^{2+} + 2e^{-}$ (2)

Cathodic reaction: $2H_2O + 2e^{-} \rightarrow + 2OH^{-} + H_2$ (3)

Products formation: $Mg^{2+} + 2OH^{-} \rightarrow Mg(OH)_2$ (4)

Alternatively, the corrosion reactions of Mg with water proceed in multiple stages as Mg first reacts with water to form MgO and hydrogen gas. The oxide layer MgO is hydrated due to reaction with water forming $Mg(OH)_2$.

$$Mg_{(s)} + H_2O_{(l)} \rightarrow MgO_s + H_{2(g)}, \Delta H^{\circ} = -360 \text{ kJ mol}^{-1} \quad (5)$$

$$MgO_s + H_2O_{(l)} \rightarrow Mg(OH)_{2(s)} + H_{2(g)}, \Delta H^{\circ} = -37.6 \text{ kJ mol}^{-1}. \quad (6)$$

The layers of MgO and $Mg(OH)_2$ should theoretically protect the surface form the alkali attack, but they are not sufficiently passive and highly unstable in the aqueous solution. The hydroxylation of MgO is shown in diagram below:

Table 2 Chemical potential of Mg & its compounds in various states at 25°C, (Perrault, 1974, 1978)

Species	Oxidation state	State	μ_o (kcal/mol)
Mg	0	Solid	0
Mg^+	+1	Ion	–61
Mg^{2+}	+2	Ion	–109
$Mg(OH)_2$	+2	Solid	–199
MgH	–1	Gas	+34
MgH_2	–2	Solid	–8
MgO	+2	Solid	–136

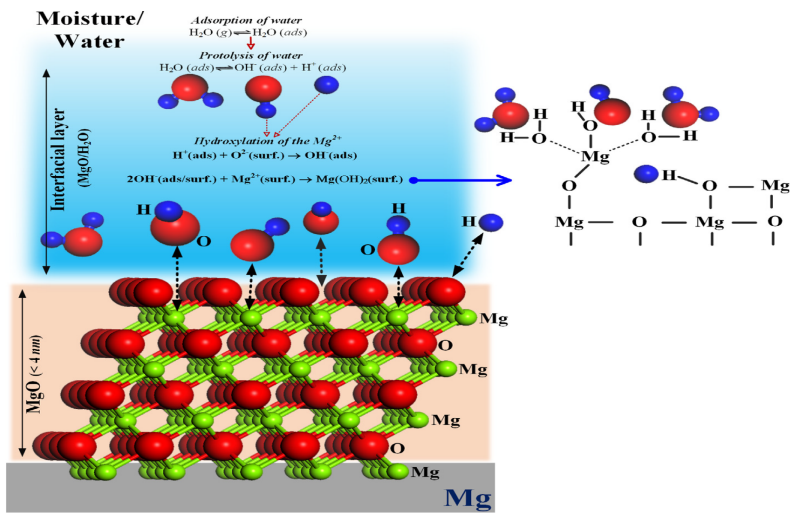

Figure 2 The hydroxylation of the surface of MgO (111) is depicted in this diagram. The software BIOVIA Materials Studio was used to visualize the atomic structures. The illustration was created using data from the document.(Shahabi, 2015).

The E-pH or Pourbaix diagram below depicts the stability regions for various species involved in the electrochemical reaction of pure Magnesium with water. The thermodynamic data for the compounds and oxide species depicted in the Pourbaix diagram was obtained by (Perrault, The potential - pH diagram of Magnesium water system,

1974). Magnesium oxidizes to MgO or $Mg(OH)_2$ for a wide range of E-pH values as shown in fig (3). The metallic Mg is relatively stable only in the region where Mg, MgH_2 and H_2 are in thermodynamic equilibrium for E-PH range shown in fig(3) Furthermore, the oxide films, MgO and $Mg(OH)_2$ are stable only in alkaline conditions with pH>10.5. Thus, the hydrated film of MgO should provide a passivating effect for metals exposed to alkaline solutions but the alkalinity required for self-passivation is not enough is most common environments. Also, the aggressive attack of chloride ions on partially protective film forms pits and increase cation dissolution. The enhancement in passivation of the oxide film with addition of RE element Neodymium and zirconium have been reported in the work (Song.Y.L, 2007), (Wang, 2008).

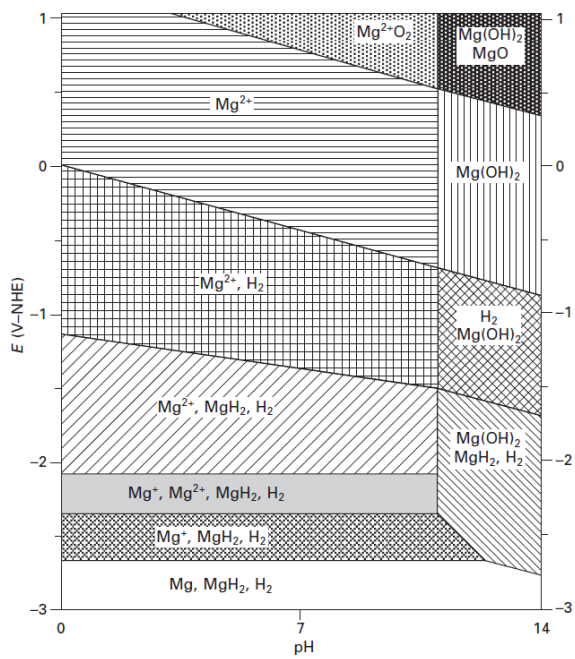

Figure 3 E-pH, Pourbaix diagram for Mg/ H_2O system (Baker, 1999), (Perrault, 1978)

The E-pH diagram is only limited in predicting corrosion behaviour and does not consider effect of chemical composition of the aqueous medium on corrosion rates. Magnesium's corrosion

performance in pure water is strongly temperature dependent. Water's resistance to corrosion decreases with increasing temperature at high temperatures, with corrosion becoming especially severe above 100°C (Ferrando, 1989).

Most acids are capable of dissolving magnesium. Magnesium dissolves quickly, even in dilute solutions of strong and moderately weak acids. Except for chromic acid and hydrofluoric acid, there are a few exceptions. The slow dissolution of magnesium in chromic acid is because it becomes passive in this acid. Because magnesium is resistant to hydrofluoric acid, an insoluble surface film of MgF_2 forms protects against further attack.
Because of the strong alkalinity of the natural hydroxide film on magnesium, the compound has a slight tendency to give up a proton to strong alkalis; thus, the film provides excellent protection even in warm solid alkali solutions that would readily attack alloys. For many years, magnesiums resistance to alkaliattack, combined with the metal's lightweight, has made it the preferred material for cement finishing tools (Henry Hu et al., 2014).

1.3.2.1. Corrosion of Mg in solutions containing various Ions

Magnesium alloys are susceptible to accelerated localized corrosion in salt solutions of varying compositions. The extent of corrosion depends on the composition of the salt solution and generally increases with increasing halide ions viz;- Chloride, bromide & iodide. Whereas chromates, phosphates and silicates inhibit corrosion rates by forming protective films, (Czerwinski, 2014). The phosphate ions $P0_4^{3-}$ and calcium ions Ca^{2+} in human body fluids form a semi protective film on the metal surface thereby forming a barrier and inhibiting corrosion. The Cl^- ions in aqueous solution are known to be detrimental to magnesium corrosion. The role of Cl^- ions in breakdown of partially protective film formed on Mg surface and dissolution mechanism of Mg in NaCl solution has been thoroughly investigated by (G.Song, 1997). The present work is focused on determining corrosion rates of selected Mg alloys in 0.9wt% salt solution and not necessarily explain the Mg dissolution mechanisms in the aqueous medium.

1.3.3. Influence of Mg corrosion products on biocompatibility:

Mg corrosion products, including released species such as (Mg^{2+}, alloying elements, gas, and OH^-) have impact on material biocompatibility. As stated, Mg^{2+} cations are generally regarded as non-toxic or even beneficial to many biological processes in the human body. Mg^{2+} ions, for example, have been shown to improve endothelial cell proliferation and migration. A recent detailed study on the influence of Mg extracts on mesenchymal stem cell fate and osteoblast genesis, on the other hand, reveals quite complex, positive, or negative results on cell differentiation via various pathways. (Frankel et al., 2017).

More research is needed to understand how Mg release affects the biological environment. The release of alloying elements from Mg alloys should also be considered. Because of the high interest in rare-earth Mg alloys, the cytotoxicity limits of these elements have been investigated. Recently, the response of endothelial cells to several Mg alloying elements (Al, Ca, Zn, Y, Dy, Nd, and Gd) as a function of ion concentration was reported; all tested elements had a dose-dependent inhibitory effect on cell viability and proliferation (Robinson et al.,2010).

Even during the early trials for Mg in medicine, the evolution of gas due to Mg corrosion was a source of concern. Assume the rate of hydrogen gas evolution due to corrosion is too fast. In that case, harmful gas pockets can form around the implant, and any method used to control the rate of Mg dissolution will also affect the rate of hydrogen gas evolution. In this context, it is worth noting that the amount of Mg corrosion is directly proportional to the amount of hydrogen gas evolving, allowing for simple, non-invasive measurement of the Mg alloy in vivo degradation rate using electrochemical gas sensors (Grillo et al., 2016)

Finally, the degradation of Mg alloys results in the formation of soluble species and the precipitation of insoluble corrosion products as surface layers (or also in the surroundings). These sparingly soluble compounds, such as Mg-hydroxide and various types of (Mg/Ca) phosphate or carbonate, can also affect biocompatibility. Insoluble

degradation products formed from pure Mg and rare earth containing Mg alloy corrosion are highly toxic to cells. By changing the surface chemistry and morphology, these surface layers will slow down degradation and influence protein adsorption and cell attachment to the Mg surface (Frankel et al., 2017).

1.3.4. Types of Corrosion on Magnesium:

1.3.4.1. Galvanic Corrosion:

Magnesium alloys are extremely prone to galvanic corrosion. Galvanic corrosion is typically manifested as intense localized corrosion of the Magnesium adjacent to the cathode. Cathodes can be external in the form of other metals in contact with Magnesium or internal in the form of a secondary solute additions or impurity phase (Froats et al., 1987). These two kinds of galvanic corrosion, external and internal, are illustrated in Fig (4):

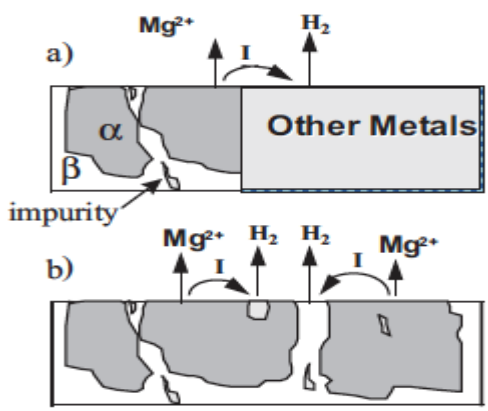

Figure 4 a) External galvanic corrosion. b) Internal galvanic corrosion. (Froats et al., 1987).

Metals with low hydrogen overvoltage, such as Ni, Fe, and Cu, serve as practical magnesium cathodes and cause severe galvanic corrosion. Metals with an active corrosion potential and a high hydrogen overpotential, such as Al, Zn, Cd, and Sn, are far less harmful. If the magnesium alloy is coupled with another metal, high purity does not protect against galvanic corrosion (Song et al.,1999).

The following factors increase the rate of galvanic corrosion: high medium conductivity, the large potential difference between anode and cathode, low polarizability of anode and cathode, the large area ratio of the cathode to anode, and a small distance between anode and cathode.

1.3.4.2. Intergranular Corrosion:

The intercrystallite attack has little effect on magnesium and magnesium alloys. Because the grain-boundary phases are invariably cathodic to the grain interior, corrosion does not penetrate inwards along the grain boundaries. Corrosion tends to concentrate in the area adjacent to the grain boundary, causing the grain to be undercut and fall out (Song et al.,1999).

1.3.4.3. Localized Corrosion:

Magnesium is prone to localized attack by heavy metal salts and chloride containing environments. According to E-Ph diagram, $Mg(OH)_2$ should be protective in strong alkaline solutions, instead a course film having small pores is developed which instantaneously provides active sites for simultaneous chloride attack and cation transport. As a result, pitting occurs in the corrosion of magnesium alloys in neutral or alkaline salt solutions. Heavy metal contamination encourages pitting attacks in general. Pits are frequently formed in MgAl alloys due to selective attack along with the Mg17Al12 network, which is followed by grain undercutting and falling out. Because magnesium corrosion is relatively insensitive to oxygen concentration differences, crevice corrosion does not occur.

An active corrosion cell that moves across a metal surface causes filiform corrosion. The anode is at the top, and the cathode is at the bottom. Under protective coatings and anodized layers, filiform corrosion occurs. Filiform corrosion does not appear in uncoated pure Magnesium. However, filiform corrosion can occur on uncoated AZ91, indicating that this alloy can naturally form a relatively resistant oxide film. The filaments are encased in an oxide film fractured by the evolving (Song et al.,1999).

1.4. Properties and Morphology of the Surface film:

Now that we have discussed about corrosion of Magnesium in aqueous solution and stability of different species in water from the Pourbaix diagram, (fig 5), it would be apt to have an overview of the surface film developed on Mg surface. The nature of film developed on Mg surface and its properties is essential to understand the corrosion reactions mentioned in section,(1.3.2) A duplex film with thin cellular layer beneath a thick porous or fibrous layer has been reported in many studies. The thin layer was found to be MgO, while the thicker layer is hydrated MgO layer which is usually porous and does not offer significant protection in alkaline environment, (Song, 2011). The hydrated layer $Mg(OH)_2$ is relatively stable as compared to MgO in strong alkaline environment, nonetheless it is still unstable in acidic, neutral, and weak alkaline solutions and does not cover the entire surface of metal substrate. Furthermore, the chloride ions aggressively attack the porous film forming corrosion pits. The thickness of the hydrated layer may increase with increased duration of exposure and could be seen in fig (7). The semi protective $Mg(OH)_2$ film has relatively large molar volume than MgO and will introduce compressive stresses within the film leading to stress rupture and micro cracks, (A. Atrens, 2018).

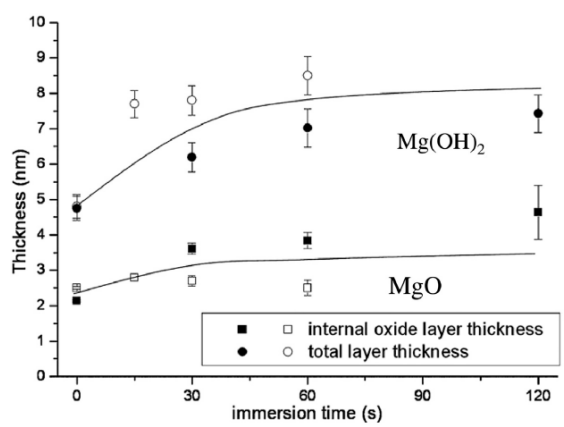

Figure 5 Formation of a thin layer of MgO covered by thicker Mg $(OH)_2$ layer as Mg is exposed to ultra-pure water (A. Atrens, 2018)

Various studies have reported columnar mixed layer of MgO-$Mg(OH)_2$ on top of the compact MgO layer, (Gernot Rother, 2015). Further research into the formation of oxide films and their allegedly dual nature is needed, and many models elucidating this dual nature could be referred to in the work (A. Atrens, 2018). Nonetheless, the isothermal calorimetry technique used in this study demonstrates enthalpy variation and energy changes associated with the formation of an oxide film, substantiating the claims.

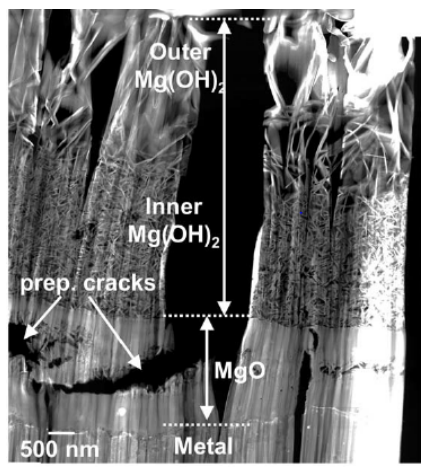

Figure 6 General film morphology observed on Mg surface exposed to aqueous medium, (Gernot Rother, 2015)

1.5. Corrosion Rate Measurement:

The corrosion rate can be measured by standard immersion testing in aqueous solution by using numerous electrochemical and non-electrochemical techniques. The discussion of electrochemical techniques is out of the scope of current research since a novel a method utilizing iso thermal calorimetry and pressure measurements was used. Thus, an overview of general non electrochemical techniques is presented in the subsequent section.

1.5.1. Weight Loss:

The weight loss method is a standard metal corrosion testing technique also considered to be a benchmark as per (M. Esmaily,

2017). This technique involves measurement of sample weight and sample size before and after exposure to the corrosive environment. The corroded film is removed prior to the weight measurement. The cleaning of the sample surface after the exposure is critical and might lead to inaccurate corrosion rate results due to insufficient or excessive cleaning. In case of Mg alloys, dilute chromic acid solution containing silver and barium nitrate is recommended for cleaning, (M. Esmaily, 2017) but a good care should be taken as this electrolyte can be hazardous.

The weight loss rate, P_W (mm/year), is determined by:

$$P_w = 2.10 * \frac{\Delta w}{At} \qquad (7)$$

where, Δw is the metallic weight loss of the specimen (measured in mg after removal of the corrosion products), A (cm^2) is the specimen area, and t (day) is the exposure period.

The weight loss testing can measure the average corrosion rates but does not provide instantaneous rate measurements which is often required as the rate changes with time.

1.5.2. Hydrogen gas collection method

The principle behind the method is evolution of hydrogen gas as magnesium dissolute into Mg^{2+} ions. According to reaction (1), One atom of Mg will react with water to form one molecule of hydrogen gas, thus the evaluation of volume of hydrogen gas evolved gives the weight loss of magnesium dissolved. This method can only be used when contribution of oxygen reduction to cathodic process in reaction (1) is neglected. In chloride containing aggressive environments like NaCl, the cathodic reaction is associated with hydrogen evolution, thus this method can be utilized. Furthermore, it gives instantaneous corrosion rate ($mm^{-1}y$) as well as average corrosion rate and is generally accurate for higher corrosion rates (>3mmy^{-1}) (A. Atrens, 2018). An inverted funnel with Mg sample placed inside a solution containing beaker is shown in the fig (7), (Min Park, 2013)

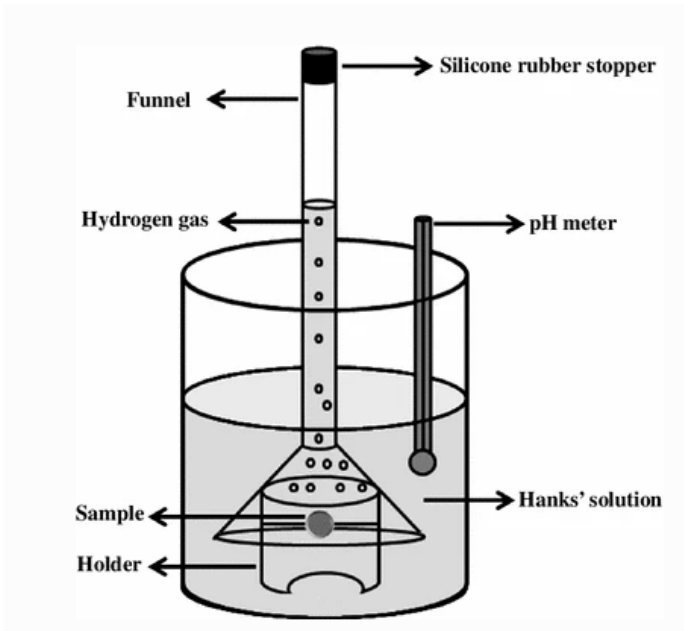

Figure 7 Hydrogen gas Collection apparatus showing inverted funnel used for measuring Mg corrosion rate by measuring volume of H2 generated in funnel, (Min Park, 2013)

1.5.3. Microcalorimetric Method

Microcalorimetric gas flow technique was developed in early 1980's to study compatibility of different materials, corrosion processes and material aging. Heat generated by individual components could be measured and thus, the extent of the reaction or rate of the reaction could be ascertained. The advantage of this technique lies in its ability to measure heat flow in range of micro watts at low temperatures.

The schematic illustration of the instrument is shown in fig (8). A corrosion rate of 0.1mm/year could be correlated to constant heat flow of approx. 20 μW. Mg powders were tested in continuous gas streams of varying composition by (Paulsson, 1989). The results obtained indicated an increase in corrosion rate with formation of $MgO/Mg(OH)_2$.Aluminium rods were tested in glass vials containing sea water by (Paulsson, 1989) using the same technique,. The results

showed an initial rise in heat flow with a sudden drop after few hours followed by stabilization. The nature of heat flow variation was attributed to the formation of protective aluminium oxide.

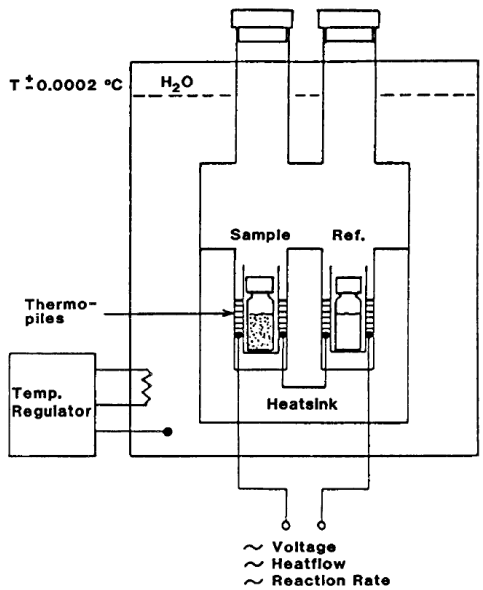

Figure 8 Microcalorimeter instrument based on large water thermostat to maintain the temperature constant. The instrument is equipped with 4 individual units having sample and reference channel. The difference in heat flow between the channels is measured by using several thermocouples connected in series.

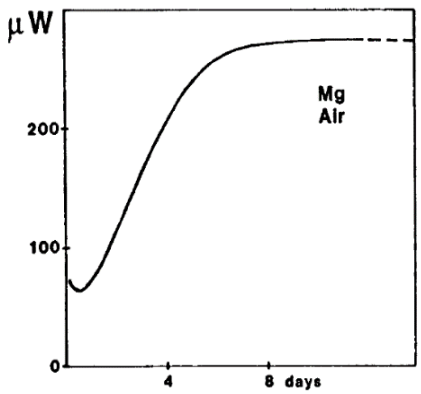

Figure 9 Rise in thermal power or heat output observed as Mg reacts with humid air indicating degradation over time, (Paulsson, 1989)

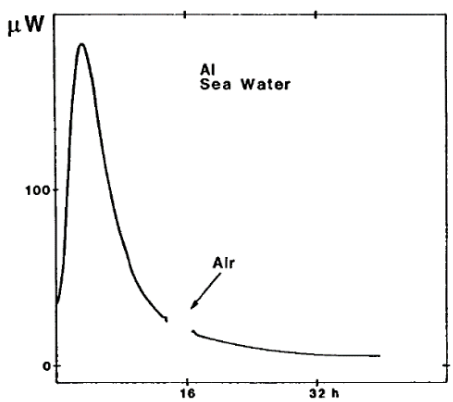

Figure 10 Degradation beahviour of Aluminium in sea water as seen from variation in thermal power or heat flow, (Paulsson, 1989)

1.5.4. Mechanical Stability of the surface films:

The Pilling-Bedworth ratio, or P-B ratio, is a useful measure for quickly assessing the potential passivating effect of a surface layer. The PB ratio is defined as the ratio of the molar volumes of a surface film to that of a bulk substrate (for example, metal):

$$R_b = \frac{V_{oxide}}{V_{metal}} \qquad (8)$$

When a surface layer has an R_{PB} of 1, it is compressed and generally stable, protecting the underlying metal from corrosion. The oxide is tensile, porous, and prone to crack formation if the ratio is less than one. The layer may form cracks and flake off, if R_{PB} is greater than 3 due to excessive compressive stresses on the layer. These cracks will then allow electrolyte to contact the metal, causing further corrosion. Mg/MgO – R_{PB} = 0.81, indicating that the MgO film is prone to cracking and thus offers little corrosion protection. In addition, MgO is water soluble. Mg, on the other hand, has an R_{PB} of 1.77. The R_{PB} for Mg -$Mg(OH)_2$ = 2.19 when the R_{PB} for Mg/MgO is divided by the R_{PB} for Mg/MgO. This suggests that it will form a strong, passivating layer. However, in this case, the PB ratio is insufficient for evaluating any potential passivating effects. $Mg(OH)_2$ crystallizes as porous networks of plate-like crystals. The metal surface does not provide adequate protection because of these pores acting as channels guiding electrolyte towards the Magnesium. Ghali (2011) defines formalized These structures are referred to as nano-flowers, and an example can be seen in fig (11).

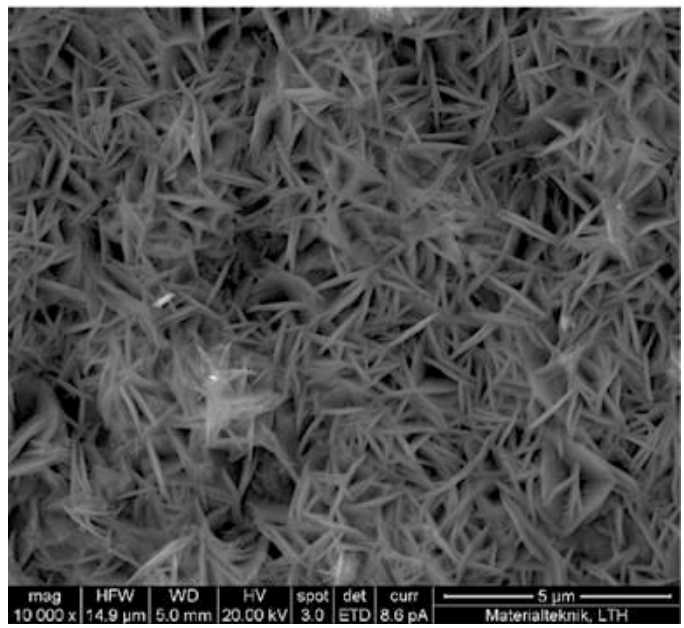

Figure 11 $Mg(OH)_2$ fibrous morphology, (D. Orlov, et al 2019)

1.6. Metallurgical Factors:

Magnesium is prone to accelerated corrosion if significant impurities are present or if it comes in contact with other metals. Because the impurities lack a natural surface film, their higher positive potential allows them to be efficient hydrogen discharge cathodes, resulting in significant micro galvanic acceleration of the corrosion rate (Song et al., 1999). As a result, even minor amounts of impurities in pure Magnesium from metals with low hydrogen over voltages, such as Fe, Ni, Co, or Cu, reduce its corrosion resistance significantly. Metals with higher hydrogen overvoltage's, such as lead, zinc, and cadmium, as well as strongly electronegative metals such as manganese and aluminium, are less hazardous in this regard. The effect of impurity and alloying elements on magnesium corrosion in a 3 percent NaCl solution at room temperature is depicted in Figure 8. Corrosion can be accelerated by Fe, Cu, and Ni, whereas Cd, Pb, Sn, and Al can significantly reduce pure Magnesium's corrosion resistance, (Tomashov, 1966).

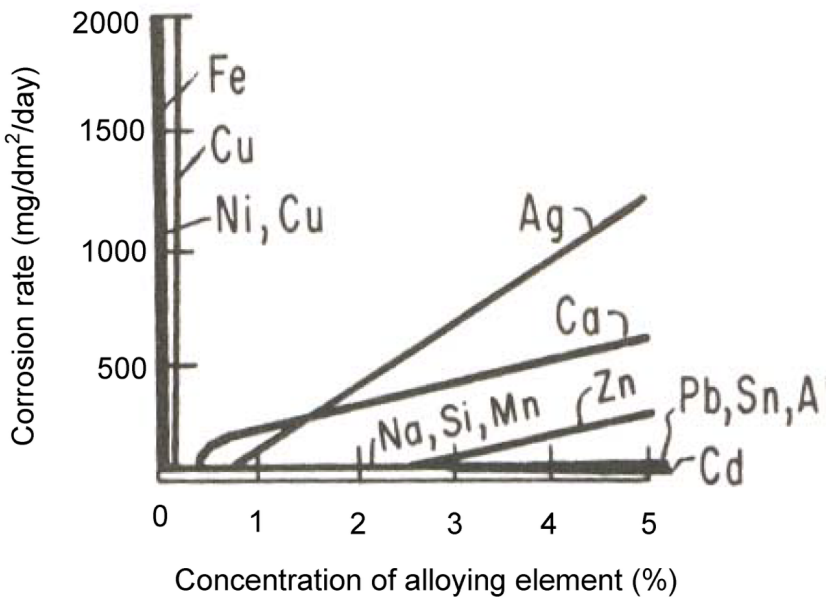

Figure 12 Effect of impurity and alloying elements on magnesium corrosion (all alloys are formed by Magnesium and the given element) in 3% NaCl solution at room temperature.

1.7. Effect of Corrosion Medium:

1.7.1. NaCl Solution:

NaCl solution is used in Mg corrosion tests for engineering and biomedical applications as general medium for corrosion tests. A simple isotonic solution is defined as NaCl solutions with concentrations of 0.85 wt. % or 0.9 wt. % that have the same osmolality as human plasma. Other concentrations of NaCl solution, such as 0.5 wt. %, 3.5 wt. %, and 0.05 M, have also been used in Mg corrosion tests but are not commonly used when testing Mg for biomedical applications (Mei et al.,2020)

Compared to other solutions, NaCl solution is a short-medium solution that usually leads to significant corrosion attacks. Two major factors influence the corrosion rate of Mg alloys in NaCl. These include a lack of buffering salts, which causes a steady rise in pH in

the solution until stabilizes and begins precipitating on the surface. The presence of chloride ions has been shown to reduce Mg corrosion resistance (Song, 2011).

To summarise, corrosion tests in NaCl solutions cannot accurately represent the complexity of real-body fluids. In comparison to more complex media, NaCl solution is the most aggressive medium that can be used to distinguish the intrinsic corrosion susceptibility properties of metallic substrates.

1.8. Heat-Treatment:

1.8.1. Influence on Grain Size:

Heat treatments are frequently used to improve mechanical properties; however, before discussing the effects of heat treatments, it is necessary to understand grain size effects. According to the Hall-Petch relationship, the mechanical properties of magnesium alloys are strongly dependent on grain size. The properties reported for any alloy and heat treatment condition are only relevant to the specific grain size of the test specimens. Fully grain-refined gravity-cast alloys should have less than 30 mm grain sizes, preferably less than 20 mm. High-temperature heat treatments, such as solution treatment (T4), can cause grain coarsening and alter mechanical properties (Gjestland et al., 2005).

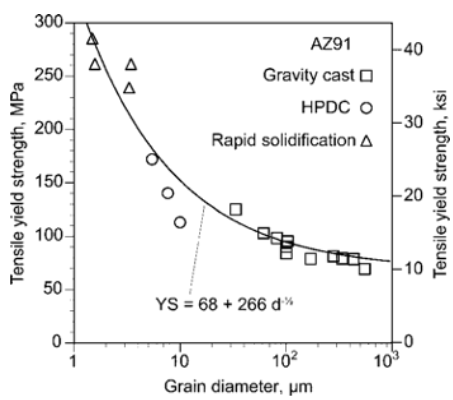

Figure 13 Shows the effect of grain size on yield strength, using data from (Gjestland et al., 2005).

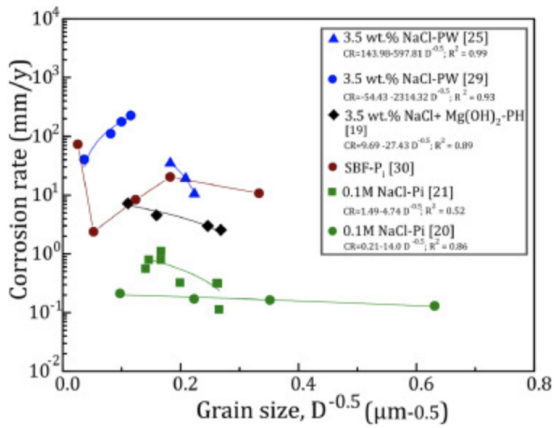

Figure 14 Effect of grain size on the corrosion rate of pure Mg (Pi, Pw and pH are corrosion rates measured by polarization, weight loss and hydrogen evolution methods, respectively) (Bahmani et al.,2020).

Fig (14) shows the corrosion rate vs. grain size of pure Mg obtained from various studies. Even in pure Mg, it appears that the single trend in corrosion rate vs grain size was not observed. While the corrosion rate increases with grain size in some cases, it decreases in others. In fact, grain boundaries are high energy sites, and corrosion begins at these locations. Annealing process increases the grain size there by reducing no of grain boundaries. Grain boundaries, assuming no flaws in the Material, should increase the corrosion rate. As a result, a single crystal material exposed to corrosion with a packed orientation like the basal plane has a very low corrosion rate (0.5 mm/y in simulated body fluid (SBF) for 1d immersion). However, by localizing the corrosion and breaking down the surface layer, adding grain boundaries and decreasing grain size increases the corrosion rate. However, in most cases, the corrosion rate has been reduced by reducing the grain size.(Bahmani et al.,2020)

As a result, in the case of single grains, such as single crystals or bi-crystals, corrosion rate increases with grain size, whereas in very fine grains (perhaps less than 50µm), corrosion rate decreases with grain size. The possibility of passivation due to the solution property, on the other hand, should be considered. Less aggressive solutions, such as 0.1 M NaCl, will most likely increase the range of passivation,

thereby increasing the grain size tolerance to provide the passivating layer.

1.8.2. Solution Heat Treatment:

The corrosion behaviour of Mg alloys is largely dictated by the composition and distribution of the secondary phase in the microstructure. The effect of these constituent phases can either be favourable or detrimental depending on their amount and distribution. Conventional casting techniques decrease the solid solubility of alloying additions and impurities within the primary matrix resulting in formation of precipitates. These precipitates are cathodic in nature with respect to magnesium and thereby form a micro galvanic couple with anodic Mg matrix. The difference in their chemical potential leads to degradation in charge carrying medium. Heat treatment re distributes the alloying elements by increasing their solid solubility in primary matrix, (Xiumin Ma, 2016). The solution heat treatment homogenizes the microstructure by decreasing amount of second phase constituents along the grains, (Z.-C. Wang, 2012).

Cast Mg-Nd alloys exhibit a separated $Mg_{12}Nd$ phase from α Mg matrix dispersed along grain boundaries, (Xiumin Ma, 2016). This phase is detrimental to Mg corrosion as it causes micro galvanic attack. At 500°C for 18 hours, the volume fraction of eutectic phase decreased; additionally, increasing the solution treating temperature to 525°C for 14 hours resulted in a homogeneous microstructure dissolving most of the eutectic compounds, (D. Wu, 2014). (Quantong Jiang, 2021) observed a decrease in degradation rate with increasing Nd content, but the corrosion mechanism shifted from galvanic corrosion to localised corrosion. $Mg_{12}Nd$ is a metastable phase that, after 96 hours of heat treatment at 500°C, transforms into the more stable $Mg_{41}Nd5$, (Easton M.A, 2012).The uniform distribution of $Mg_{41}Nd_5$ phase which has negative open circuit potential as compared to α Mg matrix showed better corrosion resistance in heat treated Mg-1.2Nd-0.5Zr alloy, (Gui-Jia Gao, 2021) Figure (15) depicts a schematic of such a heat treatment cycle for alloy N (Gene Mathers. n.d.).

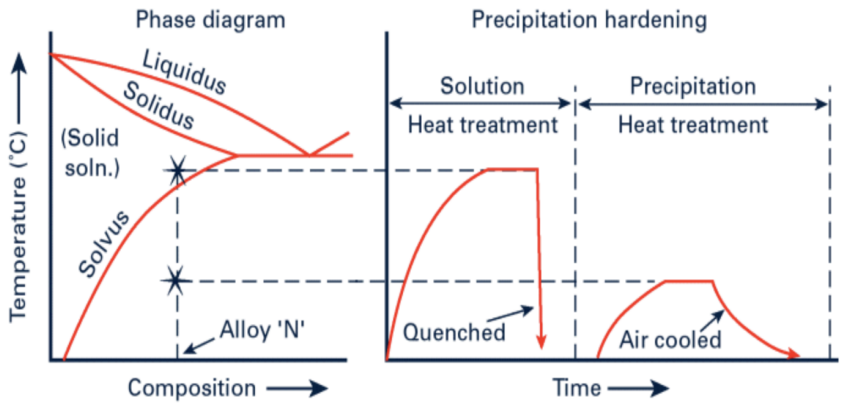

Figure 15 Schematic Phase diagram showing decreasing solubility of B in A and heat treatment cycle (Gene Mathers. N.d.)

The atoms of the alloying element, the solute, are randomly distributed throughout the matrix of the solution heat-treated metal. Still, once the temperature is raised, precipitates begin to form through a nucleation and growth process. Solute atoms begin to cluster together at relatively low temperatures and on a short timescale to form extremely small and finely dispersed precipitates known as Guinier-Preston (GP) zones. The GP zones are coherent, meaning they have the same crystal structure as the solvent metal. They do, however, distort the crystal lattice, the framework on which the atoms are arranged. This makes it more difficult for dislocations to move through the lattice. It is dislocation movement that allows the metal to deform; thus, tensile strength and hardness increase, while ductility and toughness decrease. As the ageing treatment continues or the temperature rises, the tensile strength rises as the precipitates grow and coarsen while remaining coherent (Gene Mathers. n.d.).

To achieve the best combination of properties, the precipitates must be evenly distributed throughout the grains of the alloy and should be of appropriate size. The temperature and/or time of ageing can obviously be changed to tailor the distribution and size of the precipitates; longer times and higher temperatures generally result in a reduction in strength but an increase in ductility, with an overaged structure having the lowest tensile strength but the highest ductility.

1.9. Analytical Techniques:

1.9.1. Isothermal Calorimeter and Pressure Measurements:

An isothermal calorimeter linked to pressure sensors is the primary analytical instrument in this project. An isothermal calorimeter comprises two chambers, one loaded with the sample and the other with a reference, as shown in figure 9. Heat is produced as a result of the corrosion process (Orlov,D et al.,2019). The calorimeter maintains a constant temperature in the sample. It references chambers, and the thermal power required to keep the temperature in the sample chamber constantly proportional to the rate of corrosion, as shown by the equation:

$$P = (dn/dt)*\Delta H \quad (9)$$

It is known from Mg corrosion that one mole of H2 is created for every mole of Mg consumed. This suggests that the formation of hydrogen gas is directly linked to magnesium corrosion. The corrosion rate of Magnesium may be connected to the pressure change rate of hydrogen gas using the ideal gas law, as shown by the equation:

$$dn/dt = (dp/dt)*(V/RT) \quad (10)$$

Where dn/dt is the corrosion rate of Magnesium, dp/dt is the pressure change rate of hydrogen gas, V is the total gas volume of the system, R is the gas constant, and T is temperature.

The advantage of this method of corrosion rate determination over traditional electrodynamic measurements, for example, is that a stable reading of the progress of the corrosion reaction can be made over time during immersion while affecting the specimen as little as possible. The corrosion rate can be calculated by collecting the produced hydrogen gas and measuring pressure changes over time (Orlov, D et al.,2019). When inserted in the calorimeter, Fig (16) displays a schematic of the entire pressure measuring system.

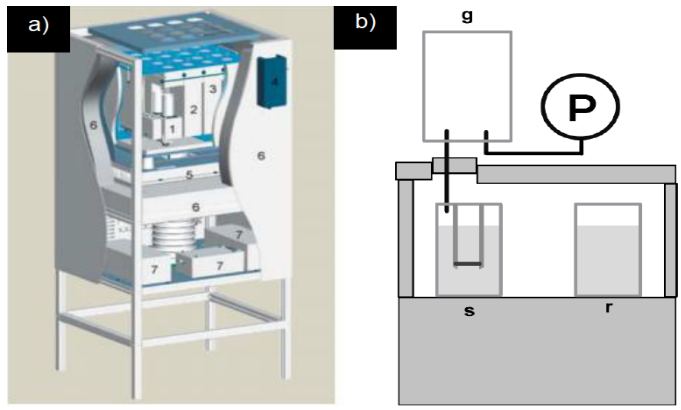

Figure 16 (a) TAM Air isothermal calorimeter. (1-3) Three of the eight calorimeter channels. (4) Temperature regulator. (5) Peltier element. (6) Insulation. (7) Data-logger and power supply (Wadsö, L. 2005). (b) The sample vial (s), the reference vial (r), and (t)

1.9.2. Scanning Electron Microscopy (SEM):

Electron microscopy is a sophisticated technique for imaging samples. Unlike tradition microscopy, which employs visible light, a scanning electron microscope (SEM), as the name implies, employs a beam of electrons that is scanned across the surface. Because electrons have a much shorter wavelength than visible light, a much higher resolution can be achieved, allowing for the imaging of very minute surface details.

There are several different types of electron detectors used in a SEM to capture the image, which affects the type of contrast seen in the final image. The two main contrasts are mass contrast (heavier elements appear brighter) and topological contrast (like regular black-and-white photography).

Most electron microscopes have X-ray detectors that can be used to identify and quantify the elemental composition of the specimen. Some energy is lost to the specimen's atom where beam interacts with it. This loss of energy is caused by electrons in those atoms being excited to a higher energy level. These electrons will then fall back to their ground state, emitting an X-ray photon in the process. The energy of that photon is characteristic of the type of element that atom is, and

it can be used to determine chemical composition of each corresponding element is proportional to the number of X-rays of a specific wavelength emitted. Energy Dispersive X-ray Spectroscopy is the term for this (EDS) (Viklund, 2020).

2. Materials and Methods:

2.1.Sample Preparation:

2.1.1. Material Used:

In this project, two binary and one ternary magnesium alloys were studied.

Specimens:

1. Mg-0.2Zr
2. Mg-0.8Nd
3. Mg-0.8Zr-0.25Nd

Table 3 Chemical composition and initial dimensions:

SAMPLE	**Chemical Composition (wt.%)**		
Material	**Zr**	**Nd**	**Mg.**
Mg-0.8Nd	---------	0.78	bal.
Mg-0.2Zr	0.2	---------	bal.
Mg-0.5Z-0.5Nd	0.25	0.74	bal.

The materials used were produced chill-cast a HZG's Magnesium in Germany. The samples were cut following the details mentioned below. Furthermore, Heat-treatment was carried out in a resistance furnace followed by quenching in ice-water, and finally, the samples were ground before immersion testing. The overview of the Cutting process, Heat-treatment and Grinding procedure are discussed below:

2.1.2. Heat-treatment:

To understand the effect of Supersaturated solid solution (SSSS) state on corrosion resistance, the As-cast was heat treated and rapidly quenched afterwards in ice water. A Table below summarises the heat

treatment temperatures and durations. A thermocouple was placed next to each specimen in the furnace, to ensuring accurate temperature control during heat treatment.

Table 4 Heat treatment

ALLOY	Mg-0.8Nd	Mg-0.2Zr	Mg-0.8Nd-0.2Zr
TEMPERATURE (℃)	525	525	525
TIME(Hrs)	10	10	10

2.1.3. Cutting-the-Sample:

Magnesium alloy billets were sectioned using a disc-blade saw. Accutom-5 by Struers was used for this purpose with 10S15 Silicon-carbide cut-off wheel as a blade.

A batch of samples from each Material was used for heat treatment to achieve the supersaturated solid solution state. Approximate dimensions of samples that were cut for heat treatment were (width x length x thickness): **10.5mm x 10.5mm x 25.0mm**.

To perform the isothermal calorimetry measurements, four specimens were needed from each material sample (i.e two from As-Cast and two from Heat-treated). Nominal dimensions of specimens that were cut for isothermal calorimetry testing, o' 'exposure' was (width length thickness's): **10mm x 10mm x 1mm**. After cutting and grinding the specimens were accurately measured and all the results were normalized by the total surface area specific to a specimen.

2.2. Surface Preparation of the Cut Specimens:

Before mounting the finished system and launching the experiment, certain final steps are required once the specimen is reduced to a 10 mm x 10 mm x 1 mm slice. Measuring the size, grinding, cleaning, and mounting are the final processes before the exposure.

The specimen were is dry-ground using 240 grit, 360 grit, 800 grit, and 1200 grit grinding papers using a Paces Technologies PENTA-5000 hand grinder. A Mitutoyo digital calliper was used to measure the specimen dimension and SHIMADZU AX120 measure the weight of each sample. Ethanol is used for final cleaning. Finally mounting of specimens is done using custom-built specimen holders.

2.3. Corrosion Media Preparation:

The corrosion properties of the sample were tested in 0.9 wt.% NaCl solution. The steps that were followed:

- A 1000 mL beaker with a stir rod was filled with deionized water to a level of approximately 900 mL.
- 9 grams of NaCl were weighed and added to the beaker in portions.
- While stirring, the beaker was filled with deionized water up to the 1000 mL gauge line.

2.4. Isothermal Calorimeter Setup:

The TAM Air from TA Instruments (previously Thermometric) calorimeter with eight independent channels was utilized in this experiment. Because the number of pressure sensors available for this project was limited, only four channels were used at a time.

The temperature of the calorimeter was set to 37°C using a PR-59 temperature controller and Lair Technologies' LT Interface Technologies matched the average body temperature in people. The calorimeter has an 8 μW detection limit (Wadsö, L. 2005).

Figure 17 Modified Isothermal Calorimeter TAM Air with control PC.

Four glass vials with a capacity of 20 mL each were prepared by filling them with 18 mL of the corrosion medium. The vials were then sealed with rubber stoppers and placed in the calorimeters' reference channel with four identical vials with 18 mL of the corrosive medium were prepared. Afterwards, specimens were placed in the vial suspended approximately in the middle of the vial. The vials were then closed with rubber stoppers, connected to a corresponding larger vial through a thin steel tube. The pressure sensors were then connected to the larger vials. The larger vial was necessary for keeping the pressure level of hydrogen gas produced during magnesium corrosion just moderately higher than atmospheric.

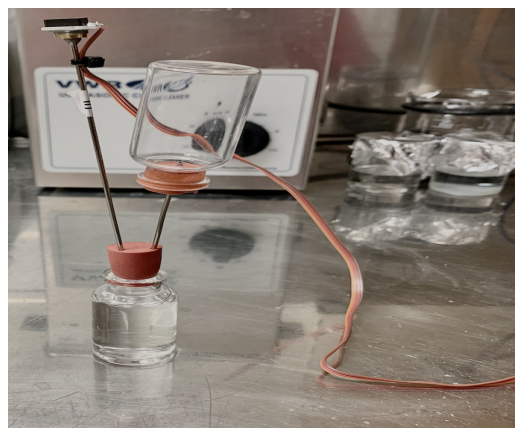

Figure 18 Experimental vial with pressure measurement setup immediately before the testing

The four assembled experimental vials with specimens were then wiped dry of any liquid residue on their surfaces before being placed in the calorimeter cell. To insulate the vials in the cell, a piece of foam was placed over them with a channel cut to allow the steel tube. Figure 15 depicts a fully loaded calorimeter. Finally, the calorimeter lid was closed, and two weights were placed on top.

Figure 19 Loaded calorimeter with pressure sensors connected.

Prior to exposure testing, the calorimeter was allowed to operate in experimental regime at least for 24 hours to allow stabilization of

all the internal components and sample environment. Final polishing and cleaning of the specimens were completed during this time.

Each vial was carefully but quickly taken from the calorimeter and a specimen mounted. During the specimen mounting, the calorimeters was kept close to calorimeter's terminal temperature disturbance. The vials were divided into two As-cast (PRES 1 and PRES 3) and two Heat-Treated (PRES 6 and PRES 8) cells. The experiment was started after all the samples were installed in calorimeter cells and connected to pressure sensors. The PicoLog PLW Recorder was used for both the calorimetric and pressure sensors data logging using a control PC.

2.5. Data Processing and Analysis:

The raw data must be processed in order to obtain important information because the PLW recorder program logs only voltage differentials. The calorimetric and pressure data were converted into quantitate process characteristics using an in-house MATLAB script which can be found in the research work of Max Viklund. Thermal power, heat flux, pressure change, pressure change rate, corrosion rate, and enthalpy variation were calculated using PLW files with calorimetric and pressure data converted to the MATLAB.

2.6. SEM Analysis:

SEM imaging was used to assess the morphology of corrosion products on the specimen surface following testing. This study employed an FEI Quanta 200 MKII microscope. Because corrosion layers were expected to be complicated in shape but generally homogeneous in content, the samples were mostly examined with secondary electrons (SE). Because corrosion products of Mg are electrical insulators, finding an area with a thin surface layer was critical to minimize charging effects distorting the image.

Figure 20 FEI Quanta 200 Scanning electron microscope (SEM).

3. Experimental Results & Discussion

A standard immersion test was conducted on selected alloy samples at 37°C inside the Isothermal calorimeter for quantitative analysis describing the corrosion behaviour. The detailed principle, methodology and procedure can be referred to in the section 1.9.1. The corrosion behaviour is analysed by multimodal technique combining pressure measurement and thermal power(J/s*). The measured quantities are normalized over the area of the samples. Furthermore, the morphology of the surface film formed over the immersion tested samples is analysed by FEI XL-30 scanning electron microscope.

The following results elucidate the effect of alloying additions and solid solution treatment in terms of corrosion rate and process kinetics.

- Thermal power per surface area (μW/mm2), measured by the calorimeter.
- Pressure variation rate (the time derivative of pressure variation, Pa/(s mm2)).
- Absolute pressure change (Pa)
- The extent of heat flow (J/mm^2)
- Corrosion rate measured in mm/year.
- Enthalpy variation(J/Kmol) calculated from corrosion rate and thermal power.

3.1. Calorimetry & Pressure measurements.

The continuous measurement of heat production rate (thermal power) and thus the energy changes associated with the corrosion reaction were successfully measured by the calorimeter equipment and furthermore, the pressure sensors mounted in the calorimeter vials gave pressure variation readings. The sensitivity of the calorimeter(<1mW) allowed us to measure the reaction heat at lower temperature (37°C). The theory behind heat conduction iso-thermal calorimetric technique could be referred to the section 1.5.3, while the first application of the technique for analysing corrosion behaviour of magnesium powders is available in the work, (Paulsson, 1989).

The pressure variation readings are consistent with the corrosion reactions (5 & 6) and supports the hydrogen evolution claim as made by, (A. Atrens, 2018).

Note: Tests were run in parallel on two samples each for as cast and heat-treated forms in 0.9wt% NaCl solution at 37°C. All result parameters are normalized over the area of samples. Corrosion rate of 0.1mm/year corresponds to constant heat flow of approx. 20mw/cm^2 of sample surface area.

AC: As cast
HT: Heat treated

Thermal power(mW/mm^2) and absolute pressure change are measured quantities, while the pressure rate change, enthalpy and heat output are calculated. A steep rise in thermal power is observed during initial couple of hours for all three samples. This initial variation signifies reaction rate kinetics can be attributed to the formation of MgO layer as bare metal surface readily reacts with the salt solution. After 2.5 hours, a drop in thermal power is observed for all three samples as well a similar variation could be seen in pressure change rate. Similar trend in process variations were observed by (Orlov) .The non-monotonic change in thermal power and its similarity with the pressure change rate elucidates various processes taking place on the Mg surface as well as confirms the 1:1(Mg/H2) relationship. The binary samples Mg-0.8Nd & Mg-0.2Zr stabilize after 5 hours while the heat-treated sample Mg-0.8Nd-0.2Zr show a continuous rise in thermal power even after 10 hours. A steady rise in thermal power and pressure change rate is seen for ternary sample Mg-08Nd-0.2Zr shown in fig(23) as the sensors get saturated after 15 hours thereby explaining sudden drop to zero. The absolute pressure variation with time for all three samples shows a single monotonic growth stage exemplifying hydrogen gas evolution as Magnesium reacts with the solution.

1 a) Mg-0.8Nd

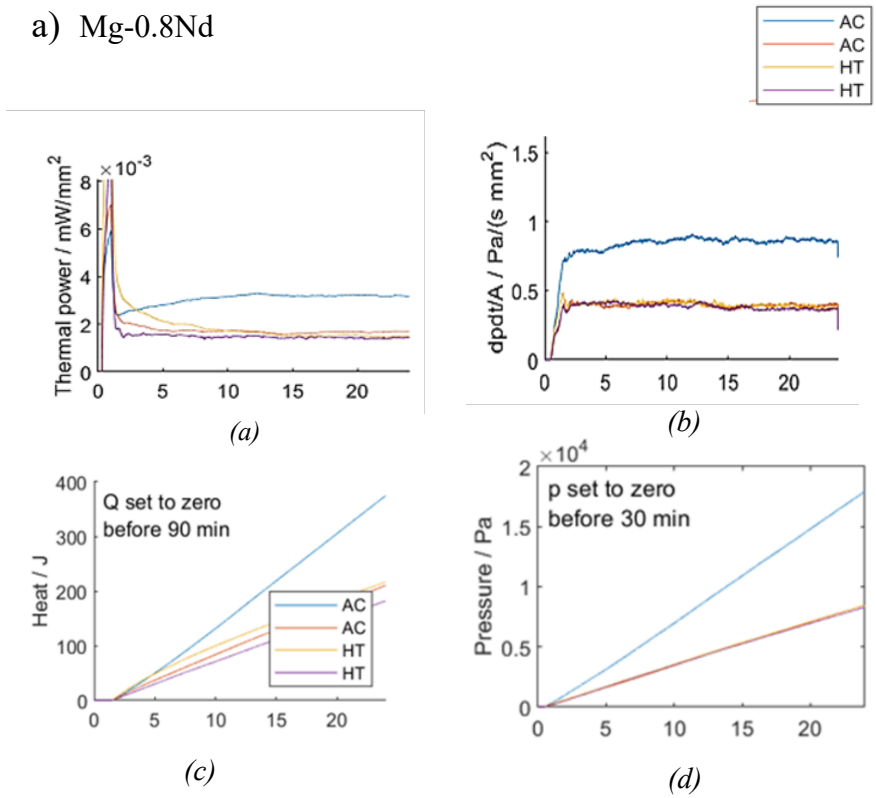

Figure 21 The results of calorimetry and pressure measurement for the Mg-0.8Nd alloy sample. Note: calculations for both as cast and heat-treated samples are included in the graphs

b) Mg-0.2Zr

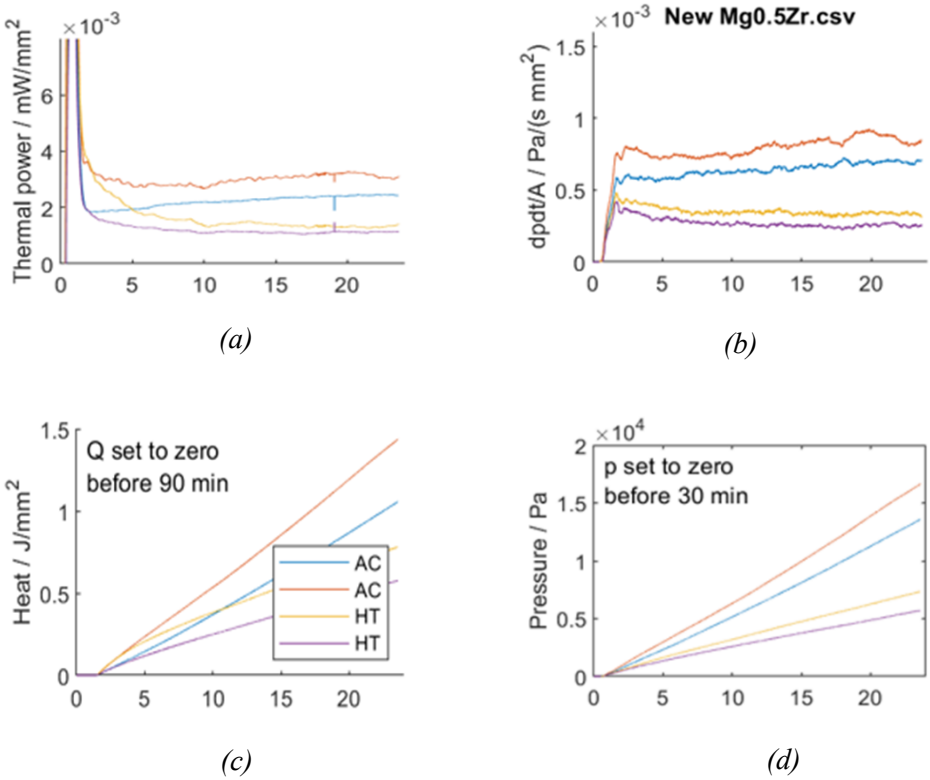

Figure 22 The results of calorimetry and pressure measurement for the Mg-0.2Zr alloy sample. Note: calculations for both as cast and heat-treated samples are included in the graphs

c) Mg-0.8Nd-0.2Zr

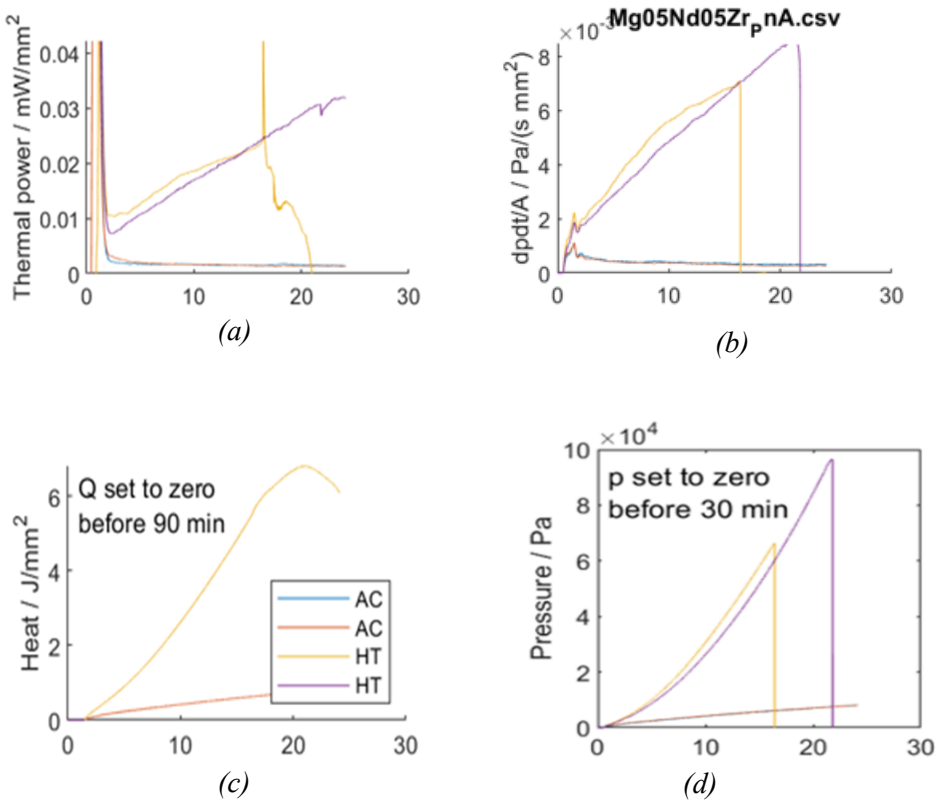

Figure 23 The results of calorimetry and pressure measurement for the Mg-0.8Nd-0.2Zr alloy sample. Note: calculations for both as cast and heat-treated samples are included in the graphs

Some key observations can be made from the Thermal power and pressure change rate graphs.

The positive deviation for thermal power over the time range confirms the reaction being exothermic. The rise in thermal power corresponds to heat energy released as the corrosion reaction takes place. The increase in thermal power accounts for maintaining constant temperature between sample and reference channel and is proportional to the rate of corrosion according to equation (8). The increase in pressure over the time or the rise in pressure change rate from fig (21-23) corresponds to hydrogen gas evolution thereby showing a consistency with the reaction (8) as shown in section (1.3.2) and substantiates the proportional relationship between hydrogen evolution and magnesium dissolution.

A passivating layer of MgO might form initially when Magnesium is immersed in solution. This layer is chemically unstable and soluble in water. The initial rise in thermal power observed for all three samples in fig (21, 22 & 23) could be correlated to the reaction of Mg with aqueous solution forming MgO , while the drop in thermal power after 2.5 hours could be the result of temperature drop as the calorimeter lid was opened for placing the samples. The influx of air creates a cooling effect thereby bringing about the change in thermal power. Furthermore, the stabilization and steady rise in the thermal power as the time proceeds indicates two stages of corrosion in magnesium alloys.

During the initial stage, the corrosion is almost uniform over the entire surface as suggested by constant thermal power reading and the steady rise seen in as cast samples could be attributed to localized attack. The localized corrosion attack increases as time proceeds and could be due to secondary particles and intermetallic phases formed by alloying additions. These solute particles dissolute in water to form hydroxide which results in increased sample surface area as they are precipitated after certain elapse in time.

A certain discrepancy is observed in fig (23a) for heat treated ternary alloy sample Mg-0.8Nd-0.2Zr in terms of steady rise in thermal power after initial drop. A stable state is not achieved as seen in other samples and it looks like the rise will continue to happen even after 24hours. The similar occurrence was observed by (Viklund, 2020), in his work on Mg-Zn alloy. A possible explanation can be cited from the work of (Viklund, 2020), although not conclusive might help in understanding the abrupt behaviour. The data obtained from Isothermal calorimeter rendered expected rise in heat output for both as cast and heat-treated alloys and the variations observed over the time range showed subtle changes happening on Mg surface as it reacted with aqueous solution.

The data as measured from pressure sensors as hydrogen gas is evolved due to reaction of Magnesium with water is depicted below for both as cast and heat-treated samples. The detailed analysis of differences observed in as cast and heat-treated samples are discussed later but these tables will provide basis for understanding of graphs shown in fig (21d, 22d & 23d).

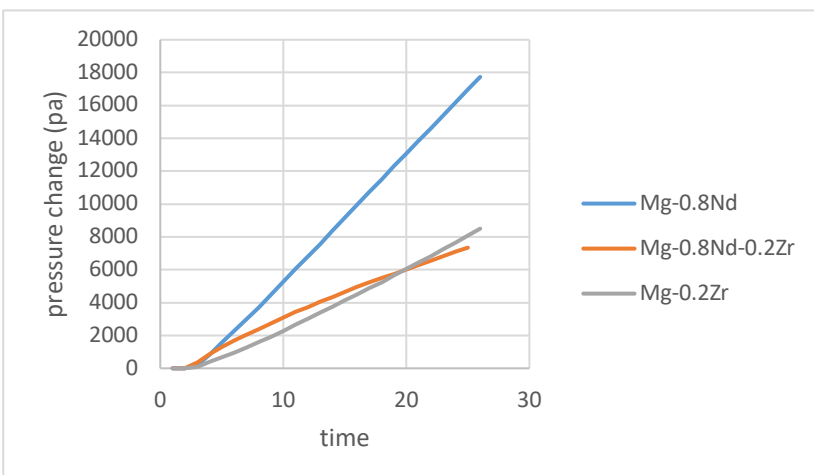

Figure 24 Pressure variation with hydrogen gas evolution for the samples(As Cast)

Table 5 Hydrogen evolution & pressure variation for as cast samples

Pressure Variation(pa) vs Time(H)			
Time (H)	Mg-0.8Nd	Mg-0.2Zr	Mg-0.8Nd-0.2Zr
1	196.4	94.22	346.79
4	2276.5	956.59	1675.81
8	5255.48	2288.82	3079.61
12	8384.95	3753.12	4353.71
16	11518.55	5247.11	5504.02
20	14636.43	6836.9	6550.49
24	17737.25	8501.2	NA

A rise in pressure variation is seen with increase in time as the reaction proceeds. After 1 hour the binary Mg-0.2Zr & Mg-0.8Nd show lower rise in pressure as compared to ternary Mg-0.8Nd-0.2Zr but after 4 hours Mg-0.8Nd shows large pressure change and continues to increase over the range of 24 hours.

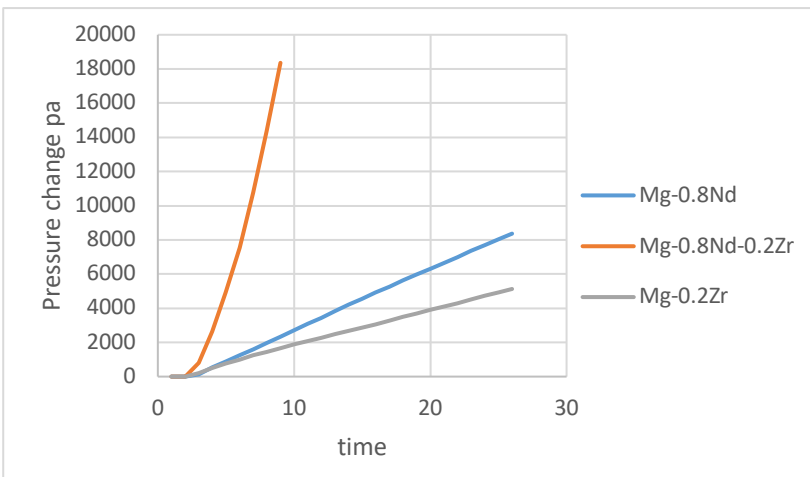

Figure 25 Pressure variation with hydrogen gas evolution for the samples(heat treated)

Table 6 Hydrogen evolution and pressure variation for heat treated samples.

Pressure(pa) vs Time(H)			
Time (H)	Mg-0.8Nd	Mg-0.2Zr	Mg-0.8Nd-0.2Zr
1	134.66	185.03	821.3
4	1235.84	1004.27	7565.4
8	2706.86	1895.07	22795.2
12	4199.82	2668.5	43137.23
16	5622.75	3482.88	-7393.51
20	7000.18	4301.7	-7468.6
24	8364.58	5127.34	NA

The negative value observed for ternary sample is due to abrupt release in pressure or saturation as the rubber stopper from the vial was blown off and can be observed.

3.2. Corrosion Rate and Enthalpy variation

The corrosion rate can be calculated from heat output(thermal power, J/sec) if a process enthalpy is known, alternatively corrosion rate can be measured from derivation of pressure rate as discussed in section (1.9.1). In the current study we have obtained corrosion rate by combination of thermal power and pressure measurement technique using iso thermal calorimeter and pressure monitoring sensors. The corrosion rate as calculated for all three samples both as cast and heat treated is presented in Eq^{n}.1

The reaction enthalpy is calculated from the ratio of thermal power(J/sec) and Mg degradation rate(mole/sec). The enthalpy change has a negative value since heat is liberated when Mg reacts with the aqueous solution to form $Mg(OH)_2$ and H_2. Also, the system is under constant pressure and the volume is increasing with the production of hydrogen gas. The enthalpy of reaction gives information about energy changes in Mg corrosion reaction at specific temperature and pressure. The experimental readings presented below can be compared with actual enthalpy of Mg corrosion reaction.

1) Mg-0.8Nd

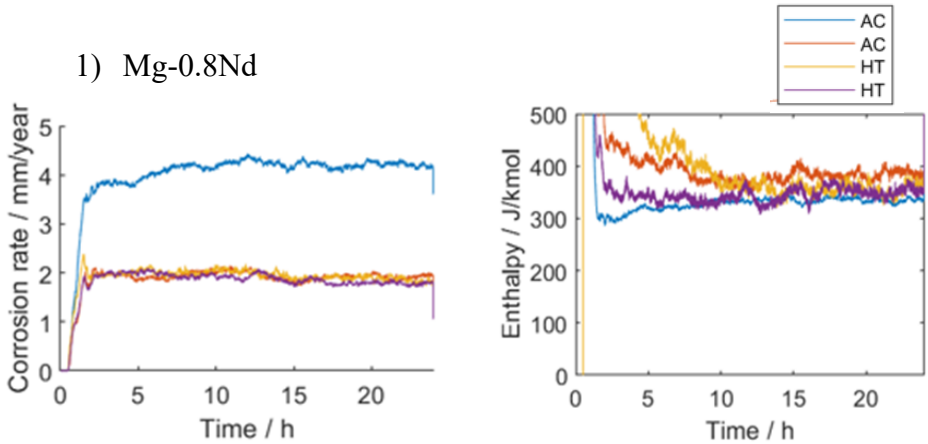

(a) *(b)*

Figure 26 Corrosion rate(mm/year) and enthalpy change (J/kmol) results for the Mg-0.8Nd alloy sample(both as cast & heat treated)

2) Mg-0.2Zr

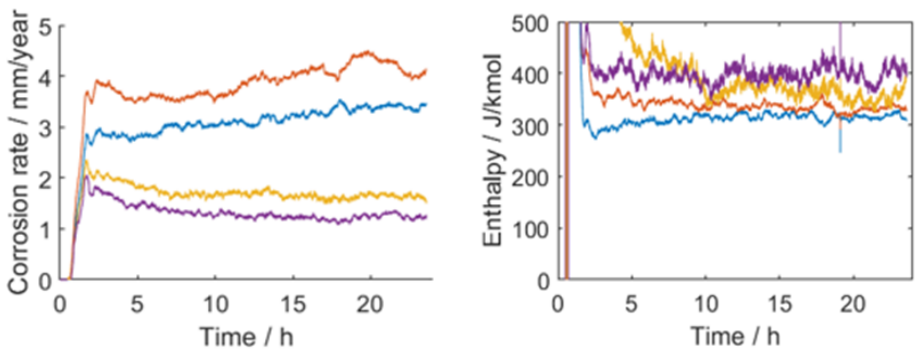

(a) *(b)*

Figure 27 Corrosion rate (mm/year) and Enthalpy change results for the Mg-0.2Zr alloy sample (both as cast and heat treated)

3) Mg-0.8Nd-0.2Zr

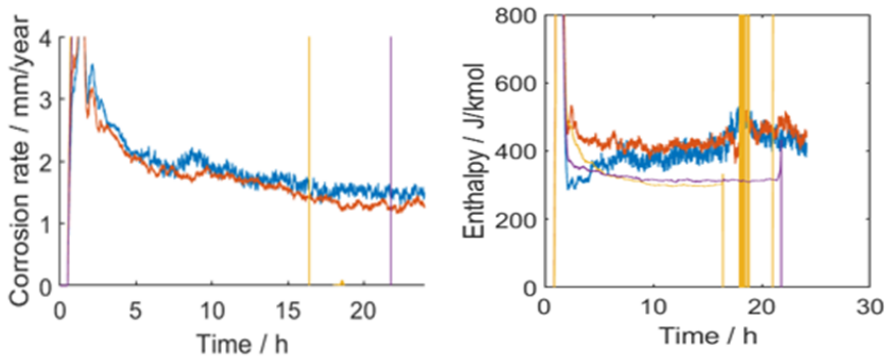

(a) *(b)*

Figure 28 Corrosion rate (mm/year) and Enthalpy change results for the Mg-0.2Zr alloy sample (both as cast and heat treated)

The graphs for corrosion rate as shown above and thermal power,(fig 26-28) are similar due to the proportional relationship mentioned in Eq^{n} (9, 10). The similarity of variation in these two quantities over the time range could be attributed to the enthalpy being constant after about 5 hours.

Both the corrosion rate and enthalpy variation show a noise. The noise in the corrosion rate graph could be due to the stability of the pressure sensors and the derivation of the pressure signal, whereas the noise observed in the enthalpy signal is related to minute process changes that occur during the reaction. The enthalpies depicted in the graphs are absolute values, but due to the exothermic reaction, they will be negative. Magnesium corrosion occurs in two stages: magnesium oxidation (MgO) and magnesium hydroxylation ($Mg(OH)_2$). In general, the formed products could be aqueous or solid, so determining their enthalpies is beyond the scope of this study. Regardless, the reaction enthalpy of the reaction thought to occur initially as Mg reacts with H_2O is -353KJmole. The experimental results are quite consistent with the previously mentioned theoretical value of enthalpy.

Enthalpy increases in as cast alloys for the first 5 hours before stabilizing in the range from 350J/Kmol^{-1} to 400 J/Kmol Whereas for

heat-treated samples, the enthalpy rises rapidly in the first 5 hours in the range of 600J/Kmol to 800J/Kmol before stabilizing in the range of 450J/Kmol to 500J/Kmol. The enthalpy change in some sample readings appears to be greater than the theoretical value mentioned above; this could be attributed to the precipitation of $Mg(OH)_2$ in the solution as it becomes saturated with $(OH)^{-1}$ ions.

Table 7 Variation in corrosion rate(mm/y) vs time(h) for as cast alloys.

Time(H)	Mg-0.8Nd	Mg-0.2Zr	Mg-0.8Nd-0.2Zr
1	1.049	0.507	1.984
4	3.836	1.58	2.104
8	4.193	1.928	2.013
12	4.316	2.017	1.767
16	4.293	2.021	1.512
20	4.32	2.228	1.459
24	4.118	2.295	NA
Corrosion rate mm/year - (as cast alloys)			

Table 8 Variation in corrosion rate(mm/y) vs time(h) for heat treated alloys.

Time(H)	Mg-0.8Nd	Mg-0.2Zr	Mg-0.8Nd-0.2Zr
1	0.742	1.015	4.65
4	2.006	1.365	14.99
8	2.032	1.194	25.066
12	2.08	1.101	30.413
16	1.922	1.195	-38.291
20	1.868	1.099	-0.14
24	1.812	1.136	NA
Corrosion rate mm/year - (Heat Treated alloys)			

The tabulated corrosion rate data in table 7 and 8 provides a concise picture of the graphs mentioned above and is used for comparative analysis between as cast and heat-treated samples. The ternary alloy Mg-0.8Nd-0.2Zr has a relatively lower corrosion rate after 24 hours, whereas the binary alloy Mg-0.8Nd showed relatively poor corrosion resistance. Solid solution heat treatment has a desirable effect on corrosion resistance as heat treated alloys are showing lower degradation rate as compared to as cast alloys albeit for ternary alloy Mg-0.8Nd-0.2Zr. The heat-treated ternary alloy is showing an abrupt rise in corrosion rate which could be attributed to the inconsistencies during the experiment. A stable variation is observed after 5 hours for heat treated binary alloys, while a gradual increase could be observed for as cast alloys after 5 hours.

3.3. Inconsistencies Observed in Experimentation

The immersion test employed in experimentation uses a relatively new technique combining iso thermal calorimetry and pressure measurement. The traditional gravimetric technique for pressure change measurement is not used here, instead pressure sensors are used which might create some stability issues and noise. Although the instrument is calibrated initially, and baseline signal is measured and subtracted from the actual experimental result still some inconsistencies were observed. The experimental trails on Mg-0.2Zr sample were repeated due to inconsistent readings as compared with literature, The details of inconsistencies are not discussed since re-trial gave expected results.

3.3.1. Effect of the alloying Elements

The corrosion performance of pure Magnesium has already been studied extensively by various authors and one such detailed analysis could be found in works of (Wadsö, 2017) while the research available on effects of selected alloying elements is quite meagre and needs to be evaluated. The influence of alloying elements on formation of protective interfaces and their interaction with surrounding body fluids is of particular interest. In the current study Neodymium and

Zirconium are investigated as viable alloying additions with the goal of achieving controlled corrosion rates.

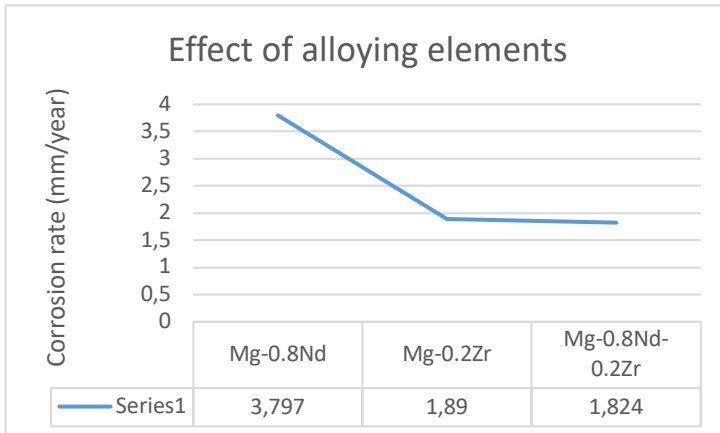

Figure 29 Average corrosion rate over 24 hours for as cast samples.

Average corrosion rate as shown fig(29) is obtained from the calculated results shown in fig (27a-28a). The binary alloy Mg-0.8Nd shows a higher corrosion rate as compared to Mg-0.2Zr and ternary Mg-0.8Nd-0.2Zr alloy. The unstable rise in corrosion rate for Mg-0.8Nd as seen in the graphs could be attributed to intense localized corrosion resulting in increased sample surface area with pits or filaments. The ternary alloy Mg-0.8Nd-0.2Zr shows a stable oxidation rate lesser than the binary alloys. The oxidation rate for Mg-0.2Zr increases initially but remains stable after 5 hours indicating uniform corrosion. The oxidation behaviour analysed in current study is compared with work done by Orlov. The results obtained by using this novel multimodal technique combining the thermodynamics as well as kinetics of the reaction with pressure measurements needs to be compared with conventional corrosion rate measurement techniques viz;- weight loss, electrodynamic polarisation studies to evaluate potency and accuracy of the test results. This was not possible due to time constraint and scope of the project.

3.3.2. Effect of Heat treatment

The alloys received were solidified by traditional casting techniques into a cylindrical billet. During Solidification, the solubility of the secondary solute additions decreases in the solid solution of primary matrix with decreasing temperature resulting in segregation of these solute atoms in form of intermetallic compounds. These intermetallic compounds or primary precipitates act as local galvanic sites creating a large potential difference relative to anodic matrix. The grain size change and re distribution of phases inside the microstructure will govern the rate of corrosion. The oxidation rate observed in Mg alloys produced by traditional casting is relatively higher than pure Magnesium and can be referred in section. Thus, one way to metallurgically control the oxidation resistance is by employing a suitable heat treatment. In the present work, all the samples are heat treated at 525°C for 10 hours inside a resistance heating furnace. The detailed methodology behind the heat treatment is mentioned in section (1.8.2)

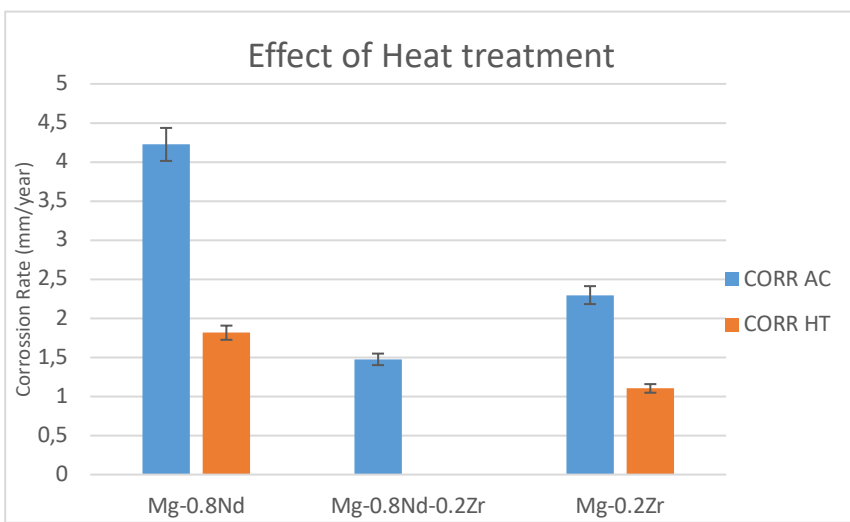

Figure 30 Difference in corrosion rate after 24 hours between as cast and heat-treated alloys.

The solid solution heat treatment has a desirable effect on corrosion resistance of binary alloys Mg-0.8Nd & Mg-0.2Zr. The ternary alloy Mg-0.8Nd-0.2Zr shows an abrupt rise in oxidation rate after heat treatment. An in-depth analysis of microstructural features with distribution of precipitates might help in evaluating this adverse effect but it could be attributed to the incipient melting due to high temperature and large time duration involved in heat treatment. In as cast from Mg-0.8Nd alloy has a higher oxidation rate relative to other samples, It might be attributed to the diversity of possible second phase reported as Mg12Nd, Mg41Nd5 and Mg24Nd which acts as cathodic sites increasing Mg dissolution. The results obtained in the current study are compared with initial work done by Orlov et al.

The concise discussion about the oxidation behaviour of all three samples in as cast and heat-treated form has been discussed by correlating graphical data and visualizing quantities for corrosion rate , pressure change derivative, thermal power & reaction enthalpy. Some noisiness was observed in the graphical data for various measured quantities, but the root cause is not same. The pressure change derivative amplifies the error or noisiness. This noisiness can be attributed to stability of pressure sensors and some unidentified signals. thus, the calorimetry results are more stable but even then, they are not completely devoid of noise. Nonetheless, the noise or the sharp variations are related to the changes happening during reaction. The Thermal power output for all three samples in as cast form is shown below.

*Figure 31 Corrosion rate(mm/year) & Pressure change rate (Pa/s*mm2) for Mg-0.2Zr alloy observed in repeatedl/new experiment.*

During the initial stages of corrosion, an increase in noise is observed for all the three samples, furthermore Mg-0.8Nd sample shows a gradual increase after 5 hours and considerable difference could be observed relative to Mg-0.2Zr and Mg-0.8Nd-05Zr alloy. The binary alloy Mg-0.2Zr & ternary alloy Mg-0.8Nd-0.2Zr show similar behaviour and might have undergone homogenous corrosion. The variation in thermal power mentioned is consistent with the corrosion rate.

3.4. Morphologies of degradation products on Mg alloy surfaces after exposure to NaCl solution

After immersion testing, all samples were removed from the calorimeter vessel, washed with distilled water, and air dried before being analysed under SEM. Before SEM analysis, a few of the samples were simply air dried without being washed. There were some interesting morphologies observed.

3.4.1. SEM images of corroded Mg-0.8Nd alloy

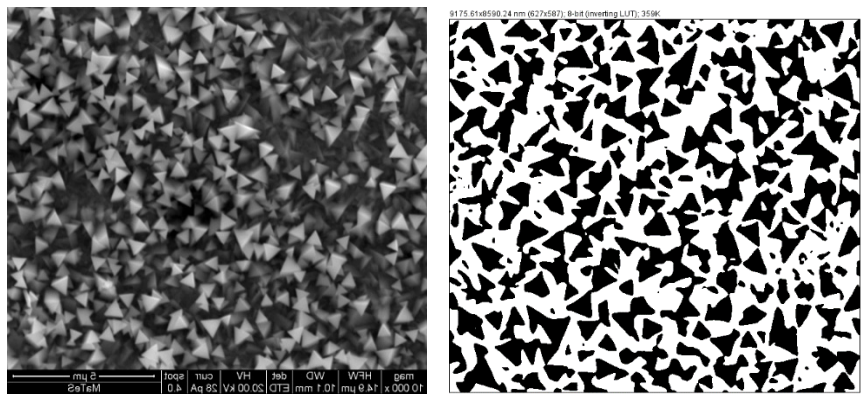

Figure 32 Mg-0.8Nd (As-cast) corroded sample. Image is analysed using Image J software.

The area of the sample is approx. 100 mm^2. 44 % of the area is covered by MgO.

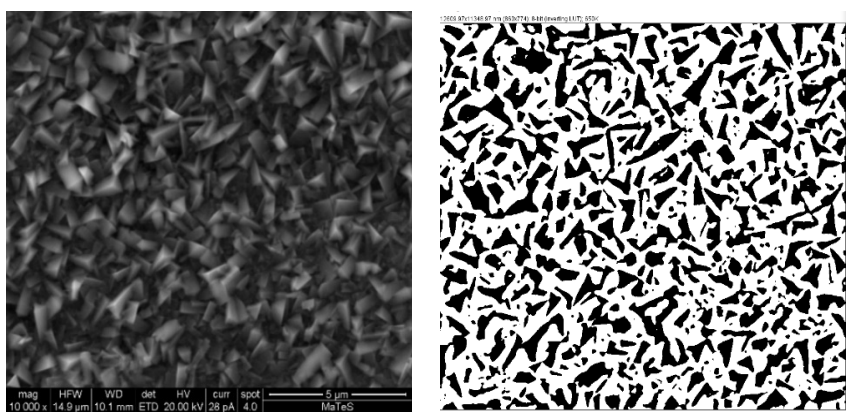

Figure 33 Mg-0.8Nd (heat treated) corroded sample. Image analysed by using Image J software

The area of the sample is approx. 100mm2 and 39.8% is covered by MgO

The micrographs shown above can be helpful in discerning morphological characteristics and effect of heat treatment after all

the samples were subjected to immersion testing for 24 hours at 37°C in 0.9% NaCl solution. Interesting prismatic features are seen in both as cast and heat-treated samples, the only difference being the size of the features and their distribution. The heat-treated sample show finer features than the as cast form. The decrease in corrosion rate might be attributed to the size of the features observed. The oxidation of Magnesium is quite complex and multiple layers are involved, moreover, the interaction of secondary solute particles and impurities also play a role in developing different morphologies. In some ways, the scope of the current project is limited because different analytical techniques are required to study elemental mapping and their composition within the observed film.

3.4.2. SEM images of corroded Mg-0.2Zr

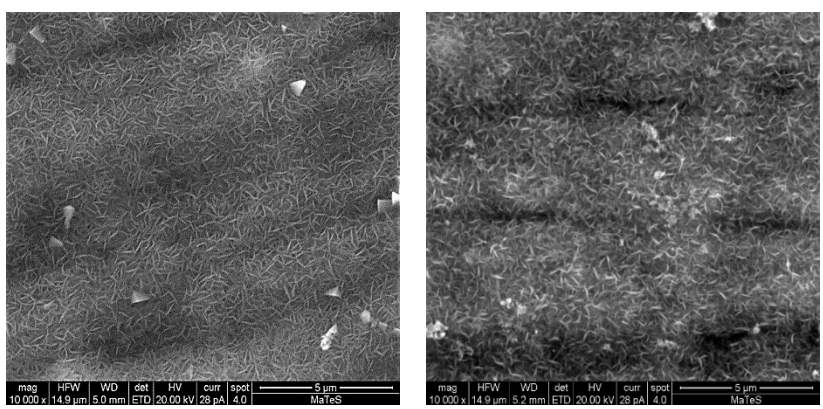

Figure 34 Mg-0.2Zr (As cast) and (heat treated) corroded sample analysed in SEM

The micrographs of Mg-0.2Zr alloy in figures (34) show a variety of morphologies. There are both prismatic features and fibrous Nano flowers visible. The drying of the sample after it was removed from the salt solution was attributed to the root cause of the change observed in these micrographs. The samples in fig (32-33)were air dried without being washed, whereas the other samples in figs (34) were washed with distilled water prior to SEM analysis. It is difficult

to predict the nature and differences observed in morphology, but a hypothesis can be developed. The fibrous Nano flowers seen on the samples in fig (34) could be caused by Mg(OH)2 decomposition to magnesium oxide (MgO) as the sample is air dried. The work of can be found with a detailed explanation for the reason (Kabunde, 1996). When cutting along one of the cleavage planes, the prismatic features may be octahedral crystals, as seen in the case of mineral periclase (MgO). Despite its low solubility in water, Mg(OH)2 has been shown in some experimental studies to dissociate to (OH)- ions as the solution's PH and alkalinity increase. The study discovered Mg(OH)2 dissociation in chloride solutions, simulated body fluids, and de-ionized water (Cheyann Lee Wetteland, 2018). MgO compact crystals can be seen in the samples shown in fig(34). In the case of air-dried samples with Nano flowers, there may be a layer of octahedral MgO crystals beneath it, but the fibrous network of flowers obscures it from view.

3.5. Comparison of Oxidation behaviour analyzed in present study with available literature.

The chemical composition of the medium and temperature are deciding factors in corrosion performance of magnesium alloys. Also, the technique involved in measuring corrosion rates might yield different results. The conventional weight loss measurement techniques give accurate results, but nothing could be interpreted about the actual changes happening during reaction and their effect on corrosion rate and products. In our attempt to Understand the oxidation behaviour of the selected samples, A novel iso thermo calorimetry and pressure measurement from hydrogen gas evolution is utilized. The results could be different from other commonly available rate measurement techniques as sometimes the leak in hydrogen gas might give inconsistent results. In present study 0.9%NaCl solution was used to mimic the chloride ions in body fluids but in actual conditions, the physiological body fluids contain calcium ions, sodium ions, phosphates and sulphates which form interfaces with the Material.

Thus, the corrosion performance in the environments containing body fluids show different oxidation behaviour as compared to samples analysed in our present work. In depth analysis of the corrosion morphologies observed in different fluids and comparison of their oxidation behaviour with the samples analysed in current study is out of the scope. Nonetheless, a short review comparing the corrosion rate of different sample compositions in different medium is discussed.

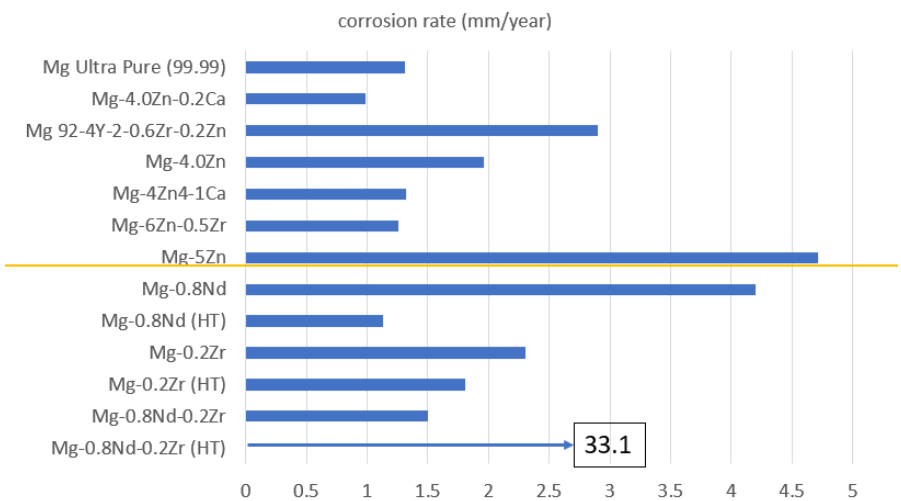

Figure 35 Corrosion rates of different Mg alloys in 0.9wt% NaCl solution.

The tabular data gives a good overview for comparison between corrosion rates observed for alloys of varying composition in same environment viz;- 0.9wt% NaCl solution. The results should not be construed as definitive because the conditions and techniques used to measure those corrosion rates differed; yet, it provides us with a preliminary image of our study in comparison to the rates shown in figure(36). Furthermore, the results obtained in the present study could be compared with previous work done by D. Orlov et al, (Orlov) as the binary alloy Mg-0.8Nd showed a marked difference in the degradation behaviour. Furthermore, the current study's results might be compared to prior work done by D. Orlov et al, (Orlov), since the

binary alloy Mg-0.8Nd shown a significant variation in degrading behaviour.

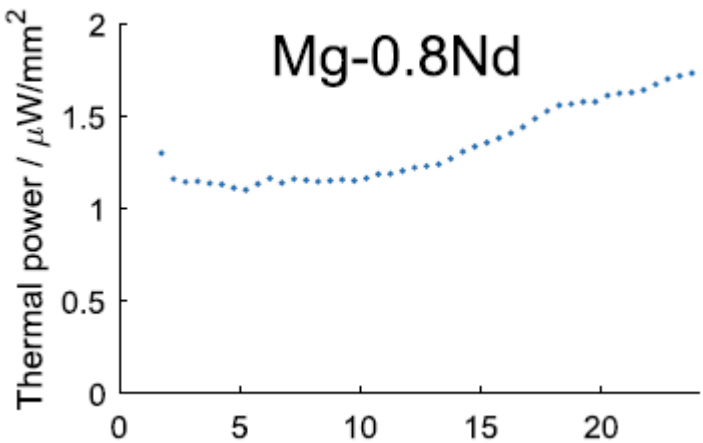

Figure 36 Thermal power variation for the Mg-0.8Nd alloy, measured using Isothermal Calorimetry, (Orlov)

The heat created by the Mg-0.8Nd alloy, as indicated in the figure above, is considerably less than the results achieved in the current investigation. Inconsistencies discovered in the study might be attributed to differences in procedure and circumstances, as well as sample preparation; nevertheless, additional examination is required.

Conclusions:

The need for developing light weight and corrosion resistant alloys for structural applications and much sensitive bio-medical field has put a great impetus on research in the field of electrochemistry and metallurgical design of new magnesium alloys. Magnesium being extremely reactive in aqueous solutions corrode at accelerated rates and generate hydrogen gas by cathodic reaction. This phenomenon also reported as negative difference effect in the literature is problematic as hydrogen evolution is proportionally increased with anodic dissolution. Although Magnesium having enriching properties for bone regeneration in bio medical application, achieving controlled oxidation rates is of paramount importance.

The present study has evaluated alloying additions of Zirconium and Neodymium as a viable option by analysing corrosion rates in dilute salt solution. Furthermore, the influence of solid solution heat treatment on oxidation rate is analysed to investigate whether metallurgical modification in microstructure could yield better performance.

The novel Isothermal calorimetry and pressure measurement technique seem to be a good option for evaluating corrosion resistance as well as thermodynamics and process kinetics of the reaction. The corrosion rate, pressure change measurements from hydrogen gas evolution, Thermal power, and Enthalpy variation for all three samples in both as cast and heat-treated forms gave a concise quantitative information for analysis, comparison, and future research.

The binary alloy Mg-0.2Zr has a better corrosion performance relative to the other alloy samples in both As-cast and Heat-treated form. The effect of solid solution heat treatment I positively observed in case of binary alloys while ternary alloy Mg-0.8Nd-0.2Zr showed abrupt rise in corrosion rate. The morphological difference observed on the corroded surfaces are due to intrinsic differences between respective corrosion reactions.

Due to time constraints, the redistribution of the main precipitate and changes in grain sizes caused by the used heat treatment were not investigated.

References:

A. A. El-Moneim, E. Akiyama, K. M. Ismail and K. Hashimoto, Corros. Sci., 2011, 53, pp 2988-2993.

A. Atrens, G.-L. S. (2018). Understanding The corrosion of Mg and Mg Alloys. *Encyclopedia of Interfacial Chemistry*, pp. 515-534.

Angrisani, N., Seitz, J.M., Meyer-Lindenberg, A. and Reifenrath, J.,

2012. Rare earth metals as alloying components in magnesium implants for orthopaedic applications. *New features on magnesium alloys*.

Bahmani, A., Arthanari, S. and Shin, K.S., 2020. Formulation of corrosion rate of magnesium alloys using microstructural parameters. *Journal of Magnesium and Alloys*, *8*(1), pp.134-149.

Cheyann Lee Wetteland, O. M. (2018). Dissociation of magnesium oxide and magnesium hydroxide nanoparticles in physiologically relevant fluids. *Journal of Nano particle Research – Springer*.

D. Wu, Y. M. (2014). Effect of heat treatment on the microstructures and mechanical properties. *Journal of Magnesium and alloys*, 20-26

Ding, Y., Wen, C., Hodgson, P. and Li, Y., 2014. Effects of alloying elements on the corrosion behaviour and biocompatibility of biodegradable magnesium alloys: a review. *Journal of materials chemistry B*, *2*(14), pp.1912-1933.

Easton M.A, G. M. (2012). The role of crystallography and thermodynamics on phase selection in binary magnesium-rare earth (Ce or Nd) alloys. *Acta Materialla*, 4420-4430.

Esmaily, M., Svensson, J.E., Fajardo, S., Birbilis, N., Frankel, G.S., Virtanen, S., Arrabal, R., Thomas, S. and Johansson, L.G., 2017. Fundamentals and advances in magnesium alloy corrosion. *Progress in Materials Science*, *89*, pp.92-193.

F. Witte, J. Fischer, J. Nellesen, C. Vogt, J. Vogt, T. Donath and F. Beckmann, Acta Biomater., 2010, 6, pp 1792-1799

F. R. Elsayed, N. Hort, M. Salgado-Ordorica, K. U. Kainer, Magnesium Permanent Mold Castings Optimization Materials Science Forum 690 (2011) 65–68.

https://doi.org/10.4028/www.scientific.net/MSF.690.65.(MagIC)

Froats, TK Aune, D. Hawke, W. Unsworth, J. Hillis, Metals Handbook, 9th ed., Vol. 13, ASM Int., Materials Park, OH 1987 , pp. 740±754. 522.

G. L. Makar and J. Kruger" "Corrosion of magnesium", International Material" "reviews, 38 (1993) pp 1"8-153.

Gene Mathers.(n.d.). *Heat Treatment of Welded Joints - Part 4*. (online)

Available at: https://www.twi-global.com/technical-knowledge/job-knowledge/heat-treatment-of-welded-joints-part-4-117. Accessed on: May 18th, 2021.

G.Song, A. (1997). *The Anodic dissolution of Magnesium in Chloride and sulphate solutions.* Pergamon Press.

Gernot Rother, L. M. (2015). Film Breakdown and Nano-Porous Mg(OH) 2 Formation from Corrosion of Magnesium Alloys in salt Solutions. *Journal of Electrochemical Society*, 162(4) C140 - C149

Ghali, E. (2011). Activity and passivity of Magnesium (Mg) and its alloys. *Corrosion of Magnesium Alloys*, pp.66-114.

Gjestland, H., Sannes, S., Svalestuen, J. and Westengen, H., 2005. Optimizing the magnesium die casting process to achieve reliability in automotive applications. *SAE transactions*, pp.67-73.

Grillo, C.A., Alvarez, F. and de Mele, M.A.F.L., 2016. Degradation of bioabsorbable Mg-based alloys: Assessment of the effects of insoluble corrosion products and joint effects of alloying components on mammalian cells. *Materials Science and Engineering: C*, *58*, pp.372-380.

Gui-Jia Gao, M.-Q. E.-L.-C. (2021). Dealloying corrosion of anodic and nanometric Mg41Nd5 in solid solution-treated Mg-3Nd-1Li-

0.2Zn alloy. *Journal of Materials Science & Technology*, 161-178

Hu, H., Nie, X. and Ma, Y., 2014. Corrosion and surface treatment of magnesium alloys. *Magnesium Alloys-Properties in Solid and Liquid States*, pp 67-108.

J. Levesque, D. Dube, M.Fiset, D. Mantovani, Adv. Mater. Process. 2004, Sept., p 45.

Klabunde, K.J., Stark, J., Koper, O., Mohs, C., Park, D.G., Decker, S., Jiang, Y., Lagadic, I. and Zhang, D., 1996. Nanocrystals as stoichiometric reagents with unique surface chemistry. *The Journal of Physical Chemistry*, *100*(30), pp.12142-12153

M. Esmaily, J. S. (2017). Fundamentals and advances in magnesium alloy corrosion. *Progress in Material Science, Elsevier*, 92-193

Mei, D., Lamaka, S.V., Lu, X. and Zheludkevich, M.L., 2020. Selecting medium for corrosion testing of bioabsorbable Magnesium and other metals–a critical review. *Corrosion Science*, p.108722.

Min Park, J. E. (2013). Polycaprolactone coating with varying thicknesses for controlled corrosion of magnesium. *Journal of Coatings Technology and Research*, 695-706.

Mirco Peron, J. T. (2017, June 25). Mg and Its Alloys for Biomedical Applications:. *MDPI*, 7(7), 252.

Nagels, J. M. (2003). Stress shielding and bone resorption inshoulder arthroplasty. *Journal of shoulder and elbow surgery*, 35-39.

Newbury D.E. (1975) Image Formation in the Scanning Electron Microscope. In: Goldstein J.I., Yakowitz H. (eds) Practical Scanning Electron Microscopy. Springer, Boston, MA. https://doi.org/10.1007/978-1-4613-4422-3_4

Orlov, D. (2019). Effect of Alloying with Rare-Earth Metals.

Paulsson, L. E. (1989). Microcalorimetric methods for corrosion rate measurement. AB Bofors, Sweden.

Perrault. (1974). The potential - Ph diagram of Magnesium water system. Journal of Electroanalytical chemistry and Interfacial electrochemistry.

Quantong Jiang, D. L. (2021). The corrosion behavior of Mg–Nd binary alloys in the harsh marine environment. Journal of Magnesium and Alloys, 292-304.

Robinson, D.A., Griffith, R.W., Shechtman, D., Evans, R.B. and Conzemius, M.G., 2010. In vitro antibacterial properties of magnesium metal against Escherichia coli, Pseudomonas aeruginosa and Staphylococcus aureus. *Acta biomaterialia*, *6*(5), pp.1869-1877.

Shahabi-Navid, M., 2015. *Atmospheric corrosion of Mg and MgAl alloys–characterization and mechanisms*. Chalmers Tekniska Högskola (Sweden).

Shi, Z. and Atrens, A., 2011. An innovative specimen configuration for the study of Mg corrosion. *Corrosion Science*, *53*(1), pp.226-246.

Song, G.L. and Atrens, A., 1999. Corrosion mechanisms of magnesium alloys. *Advanced engineering materials*, *1*(1), pp.11-33.

Song, G. and Song, S., 2007. A possible biodegradable magnesium implant material. *Advanced Engineering Materials*, *9*(4), pp.298-302.

Song, G. (2011). Corrosion electrochemistry of Magnesium (Mg) and its alloys. *Corrosion of Magnesium Alloys*, pp.3-65.

Staiger, M., Pietak, A., Huadmai, J. and Dias, G. (2006). Magnesium and its alloys as orthopaedic biomaterials: A review. Biomaterials, 27(9), pp.1728-1734.

Tamai, H., Igaki, K., Kyo, E., Kosuga, K., Kawashima, A., Matsui, S., Komori, H., Tsuji, T., Motohara, S. and Uehata, H., 2000. Initial and 6-month results of biodegradable poly-l-lactic acid coronary stents in humans. *Circulation*, *102*(4), pp.399-404.

Tomashov, N.D., 1965. Theory of corrosion and protection of metals. *1966, 672 P. THE MACMILLAN COMPANY, 60 FIFTH AVENUE, NEW YORK 10011*.

Tomashov, N.D., 1965. Theory of corrosion and protection of metals. *1966, 672 P. THE MACMILLAN COMPANY, 60 FIFTH AVENUE, NEW YORK 10011*.

Viklund, M., 2020. Degradation of model biomedical Mg alloys in aqueous media.

W. A Ferrando" "Review of Corrosion and Corrosion Control of Magnesium Alloys and Composites", Journal of Materials Engineering, 11 (1989) p" "99-313

Wadsö, L 2005' 'Applications of an eight-channel isothermal calorimeter for cement hydration studies, Cement International, vol. Jg. 3, no. Nr 5, p '.'94-101.

Wadsö, L., Hort, N. and Orlov, D. (2019). Effect of Alloying with Rare-Earth Metals on the Degradation of Magnesium Alloys Studied Using a Combination of Isothermal Calorimetry and Pressure Measurements. *The Minerals, Metals & Materials Series*, pp.121-126

Wang, H. Y. (2008). Influence of cerium on passivity behavior of wrought AZ91 alloy. Electrochemica Acta

Witte, F. (2010). The history of Bio degradable magnesium implants. Acta Biomaterialia.

Wolffe, J. (1986). The Law of Bone Remodelling. Heildelberg: Springer.

Wetteland, C.L., de Jesus Sanchez, J., Silken, C.A., Nguyen, N.Y.T., Mahmood, O. and Liu, H., 2018. Dissociation of magnesium oxide and magnesium hydroxide nanoparticles in physiologically relevant fluids. *Journal of Nanoparticle Research*, *20*(8), pp.1-17.

Xiumin Ma, Q. J. (2016). Effect of Heat Treatment on Corrosion Behaviors of Mg-5Y-1.5Nd Alloys. International journal of Electrochemistry, 9.

Z.-C. Wang, L. Y.-L. (2012). Effect of additives and heat treatment on the formation and performance of and heat treatment on the formation and performance of electroless nickel boron plating on AZ91D Mg alloy. Journal of Electrochemical Society, D406-D412.

4. Annex A: Solubility data for Binary Mg alloys :

Table 6.1 Solubility data for binary magnesium alloys

Element	at.%	wt%	System
Lithium	17.0	5.5	Eutectic
Aluminium	11.8	12.7	Eutectic
Calcium	0.82	1.35	Eutectic
Scandium	~15	~24.5	Peritectic
Titanium	0.1	0.2	Peritectic
Manganese	1.0	2.2	Peritectic
Zinc	2.4	6.2	Eutectic
Gallium	3.1	8.4	Eutectic
Strontium	0.03	0.11	Eutectic
Yttrium	3.75	12.5	Eutectic
Zirconium	1.0	3.8	Peritectic
Silver	3.8	15.0	Eutectic
Cadmium	100	100	Complete SS
Indium	19.4	53.2	Peritectic
Tin	3.35	14.5	Eutectic
Lanthanum	~0.04	~0.23	Eutectic
Cerium	0.1	0.5	Eutectic
Neodymium	~1	~3	Eutectic
Samarium	~1	~6.4	Eutectic
Gadolinium	4.53	23.49	Eutectic
Terbium	4.6	24.0	Eutectic
Thulium	6.3	31.8	Eutectic
Ytterbium	1.2	8.0	Eutectic
Gold	0.1	0.8	Eutectic
Thallium	15.4	60.5	Eutectic
Lead	7.75	41.9	Eutectic
Bismuth	1.1	8.9	Eutectic
Thorium	0.52	4.75	Eutectic

Annex B: General Effects of elements used in magnesium alloys:

Table 6.2 General effects of elements used in magnesium alloys

Alloying element	Melting and casting behavior	Mechanical and technological properties	Corrosion behavior I/M produced
Ag		Improves elevated temperature tensile and creep properties in the presence of REs	Detrimental influence on corrosion behavior
Al	Improves castability, tendency to microporosity	Soli solution hardener, precipitation hardening at low temperatures (<120°C)	Minor influence
Be	Significantly reduces oxidation of melt surface at very low concentrations (<30 ppm), leads to coarse grains		
Ca	Effective grain-refining effect, slight suppression of oxidation of the molten metal	Improves creep properties, ideal for developing biomaterials	Detrimental influence on corrosion behavior
Cu	System with easily forming metallic glasses, improves castability		Detrimental influence on corrosion behavior, limitation necessary
Fe	Magnesium hardly reacts with mild steel crucibles		Detrimental influence on corrosion behavior, limitation necessary
Li	Increases evaporation and burning behavior, melting only in protected and sealed furnaces	Solid solution hardener at ambient temperatures, reduces density, enhances ductility	Decreases corrosion properties strongly, coating to protect from humidity is necessary
Mn	Control of Fe content by precipitating Fe–Mn compound, refinement of precipitates	Increases creep resistance	Improves corrosion behavior due to iron control effect
Ni	System with easily forming metallic glasses		Detrimental influence on corrosion behavior, limitation necessary
REs	Improves castability, reduces microporosity	Solid solution and precipitation hardening at ambient and elevated temperatures, improve elevated temperature tensile and creep properties	Improves corrosion behavior
Si	Decreases castability, forms stable silicide compounds with many other alloying elements, compatible with Al, Zn, and Ag, weak grain refiner		Detrimental influence
Sn	Increases ductility	Solid solution hardener, less effective in precipitation hardening	Detrimental influence on corrosion behavior
Sr	Increases castability, reduces microporosity	Improves creep resistance, ideal for developing biomaterials	Detrimental influence on corrosion behavior
Th	Suppresses microporosity	Improves elevated temperature tensile and creep properties, improves ductility, most efficient alloying element	
Y	Grain-refining effect, increases ignition temperature of molten metal	Improves elevated temperature tensile and creep properties	Improves corrosion behavior
Zn	Increases fluidity of the melt, weak grain refiner, tendency to microporosity	Precipitation hardening, improves strength at ambient temperatures tendency to brittleness and hot shortness unless Zr refined	Minor influence, sufficient Zn content compensates for the detrimental effect of Cu
Zr	Most effective grain refiner, incompatible with Si, Al, and Mn, removes Fe, Al, and Si from the melt	Improves ambient temperature tensile properties slightly	

Modified from Neite, G *et al.*: Magnesium-based alloys in materials science and technology: a comprehensive treatment. Cahn, RW, Haasen, P and Kramer, EJ (Eds.), Vol. 8, *Structure and Properties of Non-Ferrous Alloys*, VCH, Weinheim, Germany, p. 113, 1994.

Annex C: Comparison of the mechanical properties of natural bone with various implant materials:

Properties	Natural Bone	Stainless Steel	Ti Alloy	Co-Cr Alloy	Magnesium
Density (g/cm^3)	1.7–2.0	7.9–8.1	4.4–4.5	8.3–9.2	1.74–2.0
Elastic modulus (MPa)	3–20	189–205	110–117	230	41–45
Tensile strength (MPa)	80–150	480–620	930–1140	900–1540	170–270
Compressive yield strength (MPa)	130–180	170–310	758–1117	450–1000	65–100
Elongation at failure (%)	1–7	30–40	8–15	30–45	6–20
Fracture toughness (MPa $m^{1/2}$)	3–6	50–200	55–115	100	15–40

Annex D: Schematic representation of the effect of grain size refinement on corrosion propagation:(Bahmani et al.,2020)